

## Homology modeling, ligand docking and in silico mutagenesis of *Neurospora* Hsp80 (90): insight into intrinsic ATPase activity

Samir S. Roy, Robert W. Wheatley, Manju Kapoor\*

Department of Biological Sciences, The University of Calgary, 2500 University Drive NW, Calgary, AB T2N 1N4, Canada

### ARTICLE INFO

#### Article history:

Accepted 21 February 2013

Available online 1 March 2013

#### Keywords:

Hsp90s  
Homology modeling  
Ligand docking simulation  
*Neurospora crassa*  
*Saccharomyces cerevisiae*

### ABSTRACT

The Hsp90 family of proteins is an important component of the cellular response to elevated temperatures, environmental or physiological stress and nuclear receptor signalling. The primary object of this work is the 80-kDa heat shock protein, a member of the Hsp90 family, from the model filamentous fungus *Neurospora crassa*, (henceforth referred to as Hsp80Nc). In contrast to more extensively characterized members of the same family, (e.g. Hsp82Sc of *Saccharomyces cerevisiae*) it exhibits a higher intrinsic ATPase activity and the ability to form hetero-oligomeric complexes with Hsp70 in the absence of co-chaperones or other ancillary factors. As unabridged experimentally derived structures of Hsp80Nc or Hsp82Sc are not available; we developed homology-based models for both of them. A structural analysis and comparison of these models was undertaken to better understand the nature of dimerization-induced changes in secondary structure and patterns of residue interaction. Our studies yielded some interesting and novel insights into the synergistic and mutually reinforcing nature of interactions between major domains of the two chains in their dimeric forms. We also evaluated the effect of residue substitutions in the 'lid' region of Hsp80Nc and Hsp82Sc on the calculated ligand-binding energy of ATP (and ADP) to their respective N-terminal domains. Our studies suggest that the higher intrinsic ATPase activity of Hsp80Nc may be attributable to differences in the residue sequences between the lid region of these two proteins.

© 2013 Elsevier Inc. All rights reserved.

### 1. Introduction

Heat shock proteins (Hsp) comprise a class of molecular chaperones, encompassing several evolutionarily conserved families, whose expression is accelerated upon exposure to elevated temperatures and other forms of environmental/physiological stress [1,2]. Their up-regulation is a critical component of the heat shock response in virtually all organisms ranging from bacteria, Archaea and plants to humans. Some families of Hsps are also important components of intracellular signal transduction pathways, including those involved in nuclear receptor signalling [3,4]. Hsps are traditionally classified according to their molecular mass (kDa) into the following families: small Hsps (<40 kDa), Hsp40, Hsp60, Hsp70, Hsp90 and the Hsp-70 related Hsp110 [1]. The smaller Hsps, including Hsp27 and Hsp20, appear to form complexes and act in concert with larger Hsps [5–8]. These large, and ATP-dependent, Hsps have been extensively investigated because of their important role in normal cellular growth and death as well as in disease processes like various types of cancer [9,10]. The activity of larger Hsps is

regulated, both positively and negatively, by interactions with a variety of ancillary factors and co-chaperones [11,12].

The Hsp90 family is one of three major families of large ATP-dependent Hsps, ubiquitous in eukaryotic and prokaryotic organisms, but apparently absent in the Archaea [13–15]. It is powered by nucleotide hydrolysis which primarily occurs inside the well-characterized nucleotide binding site within its N-terminal domain (NTD) [16–18]. In addition a secondary nucleotide binding site has been demonstrated in its C-terminal domain (CTD) [19–21]. Furthermore, Hsp90 is implicated in classical Hsp functions such as protein folding/triage as well as more physiological pathways related to cell signalling and growth [22,23]. It accomplishes these diverse functions by forming complexes with other molecular chaperones including large Hsps (e.g. Hsp70), smaller Hsps (e.g. Hsp27) and other proteins mediating nuclear receptor signalling and cytokine regulation [9]. A number of protein co-chaperones that interact with Hsp90—exemplified by Aha1 (an activator) and Sti1 (a repressor)—also regulate its activity [11]. Transition metal oxyanions, such as vanadate, also interact with Hsp90 and modulate its ATPase activity, although their physiological function is unclear [24]. The extensive involvement of Hsp90 in cell repair, proliferation and response to nuclear hormones makes it a potential target for development of new anti-cancer drugs. Preclinical studies suggest that specific Hsp90 inhibitors

\* Corresponding author.

E-mail address: [mkapoor@ucalgary.ca](mailto:mkapoor@ucalgary.ca) (M. Kapoor).

(i.e. Geldanamycin and derivatives) show promise in the treatment of certain types of cancer [25].

The object of this work is the 80-kDa heat shock protein, a member of the Hsp90 family, from the model organism, the filamentous fungus *Neurospora crassa*, henceforth referred to as Hsp80Nc [26,27]. Hsp90 family members in lower eukaryotes (yeasts, fungi and protists) are generally characterized by molecular masses ranging from ~80 to 83 kDa. Hsp80Nc, like other Hsp90s, contains three major structurally distinct domains; a ~25-kDa N-terminal domain (NTD) linked via a 'charged', species-specific linker to the ~40-kDa Middle domain (MD) which is connected, via a short linker, to a ~12-kDa C-terminal domain (CTD) culminating in a species-specific tail region. The amino acid sequence of Hsp80Nc displays significant homology to Hsp90s from other eukaryotic species such as *S. cerevisiae* and *H. Sapiens*, pairwise percentage sequence identity being 71.7% with the former and 60.5% with the latter [27]. The maximum degree of sequence and, therefore, potential structural homology between eukaryotic Hsp90s is observed in residues comprising the three major domains.

Contrasted with corresponding members of this family in other eukaryotic species—i.e. human, chicken and yeast—Hsp80Nc exhibits a higher intrinsic ATPase activity ( $K_m = 5.1 \mu\text{M}$ ;  $k_{cat} = 1.12 \text{ min}^{-1}$ ) without intervention by cochaperones or client proteins [28]. For instance, the reported intrinsic ATPase activities of Hsp90 proteins of Human cells ( $K_m = 840 \mu\text{M}$ ;  $k_{cat} = 0.089 \text{ min}^{-1}$ ) and chicken ( $K_m = 300 \mu\text{M}$ ;  $k_{cat} = 0.02 \text{ min}^{-1}$ ) are considerably lower; the reported  $K_m$  values for yeast Hsp90s vary from 100 to 830  $\mu\text{M}$  and  $k_{cat}$  from 0.05 to 0.4  $\text{min}^{-1}$  [16,29]. Upon addition of the cognate glucocorticoid receptor protein to human Hsp90, a decrease of  $K_m$  to 500  $\mu\text{M}$  and increase of  $k_{cat}$  by 13-fold to ~1.16  $\text{min}^{-1}$  was recorded [30]. These values are similar to the intrinsic ATPase activity of Hsp80Nc—unassisted by activating cochaperones. Another distinguishing feature of Hsp80Nc is a direct physical interaction with purified Hsp70 of *N. crassa* to form hetero-oligomeric complexes, documented by affinity chromatography, ELISA (Enzyme-linked immunosorbent assays) using specific polyclonal antibodies, inter-protein chemical cross-linking and SPR (surface Plasmon resonance) measurements [31,32]. The structural and mechanistic basis of its higher intrinsic activity and hetero-oligomerization is not well understood, because of the lack of an experimentally derived structural model of the native, full-length Hsp80Nc. We have attempted to address this issue by building homology-based models of the monomeric and dimeric forms of Hsp80Nc for the purpose of comparing them to equivalent molecular models of Hsp82Sc. Since all known experimentally derived structures of Hsp90s, including those of Hsp82Sc, are derived from inactive truncated constructs, it is difficult to make any meaningful comparison between homology-based models of Hsp80Nc and experimentally derived structures of Hsp82Sc constructs [33]. It was therefore deemed necessary to construct unabridged homology-based models of Hsp82Sc, preferably with the same methodology and tools used for Hsp80Nc models.

We are aware that several research groups have previously constructed homology-based models of full length versions of Hsp90s [34]. These were created with the objective of reproducing the overall structure of Hsp90 dimers and monomers as evident using cryo-electron microscopy [35]. The current state of understanding of structural changes during the process of Hsp90 activation and dimerization is largely based on extrapolation of data obtained through indirect structural methods (Electron Microscopy, Circular Dichroism, 2D NMR and H-D exchange) onto X-ray crystallography based molecular models. The sum of available information about structural changes during Hsp90 activation does, however, reveal some internal inconsistencies. For instance, studies using Circular Dichroism (CD) spectroscopy have demonstrated that Hsp90s do undergo measurable conformational changes during activation

and in the presence of regulating co-chaperones [36,37]. Electron microscopy has also shown that Hsp90s exhibit significant shape shifts upon activation, primarily related to changes in the relative position of the major domains [35,38]. It also appears that nucleotide binding at the N-terminal nucleotide binding site unmasks another nucleotide-binding site in the C-Terminal domain [39]. However, experiments utilizing 2D NMR, in contrast, do not reveal large post-activation structural changes amongst the majority of residues constituting the main domains in Hsp90s [40]. Binding of various co-chaperones also appears to have rather modest effects on the 2D NMR spectra of Hsp90s in spite of their considerable effects on activity [41,42]. The apparent discrepancy between experimental data obtained via various indirect methods is best reconciled if we assume that most large structural changes during Hsp90 activation primarily occur in the numerical minority of residues (10–15%), constituting the inter-domain linkers and other flexible regions, as opposed to the bulk of residues (85–90%) comprising the major domains. However, one of the persistent issues in modeling full-length Hsp90s is the lack of experimentally derived structures for residues in these very regions, namely, the 35 to 60 residues long "charged" linker and the 30 to 35 residues long "C-terminal tail". As mentioned in the foregoing, these regions are excluded from, or modified, in constructs that have been used for structural determination by X-ray crystallography since they appear to hinder crystal formation, even though their presence is essential for the normal biological functioning of Hsp90s [43,44]. Hence we decided to build models of both regions, based on indirect experimental evidence, for incorporation in models of full-length Hsp80Nc and Hsp82Sc.

There is convincing experimental evidence that mutations in the 'lid' region of Hsp82Sc alter its levels of intrinsic ATPase activity [45]. It is however not clear if, or how, differences in residue sequence between the 'lid' region of Hsp80Nc and Hsp82Sc contribute to their relative levels of intrinsic activity. We propose to address this question by assessing the ligand-binding energy of ATP and ADP in molecular models of Hsp80Nc and Hsp82Sc, together with versions in which the lid sequence of each protein is progressively altered to resemble the other. Ligand binding energy values are prime indicators of specificity and "fit" of the ligand in the receptor pocket with a direct impact on the efficiency of the catalytic process.

This communication entails: (i) the construction and comparison of multiple homology-based models of Hsp80Nc and Hsp82Sc; (ii) de novo modeling of inter-domain linkers and other flexible regions of both Hsp80Nc and Hsp82Sc, based on our extrapolations of available experimental data; (iii) a comparison of Hsp80Nc and Hsp82Sc models to better understand the nature of activation-induced structural changes; (iv) analysis of the effect of residue substitutions in the 'lid' region of Hsp80Nc and Hsp82c on the calculated ligand-binding energy of ATP and ADP.

## 2. Materials and methods

### 2.1. Molecular modeling software

The bulk of the work described in this communication comprises the extensive use of computational chemistry based methods. Therefore considerable effort was spent in selecting the most optimal program for each major part of our study. However we realized that using a different program for each part of the project had an undesirable effect on the overall workflow. Initially, minor problems such as partial incompatibility between the input and output file formats of various specialized programs were encountered. The most serious obstacle to the sequential use of specialized stand-alone programs is that each one seemingly uses its own

version or interpretation of well-known molecular mechanics force-fields. Consequently, the outputs of one program necessitate a brief energy re-optimization before use as one of the inputs for another one. Since our study involved calculation of the binding energy for ligands docked into homology-based models of Hsp80Nc and Hsp82Sc, the use of stand-alone programs for each part of the project would have created disruptions in the workflow. We opted to use a well documented general-purpose molecular modeling suite, MOE (Molecular Operating Environment), specifically MOE 2008.10 on computers with dual and quad core processors and at least 2GB of RAM running either Windows XP Pro-SP3 or Windows 7 HP-SP1 [46]. It was deemed satisfactory for all parts of the project as it implemented a current version of the well-characterized MMFF94 force field [47].

## 2.2. Homology modeling procedure

Default procedure and settings for creating homology-based models of proteins, as implemented in MOE 2008.10, were used to create models of Hsp80Nc and other selected members of the Hsp90 family. Publicly available structures (\*.pdb format) and residue sequences (\*.fst format) for all Hsp90 proteins studied were downloaded from NCBI [48]. Alignment between multiple sequences (for alignment and homology studies) and sequences and structural templates (homology-based modeling) were performed with the BLOSUM62 matrix using the default sequence alignment module in MOE [49].

The homology modeling procedure in MOE consists of the following steps: (1) alignment of residues from the target sequence and structural template; (2) generation of initial partial structures where Cartesian coordinates from identical residues in the structural template are conserved; (3) Boltzmann-weighted randomized sampling of non-conserved and partially conserved residues consisting of a data-collection step and a model building step. Data collection involves collection of backbone fragments from a high-resolution structural database, and assembly of alternative side chain conformations for non-identical residues, derived from an extensive residue rotamer library. During model building, 10 independent models were constructed based upon loop and side chain placements scored by a contact energy function. The final model was a best energy minimized intermediate model.

## 2.3. Ligand docking procedure

The Site Finder module in MOE was used to place dummy atoms into the active site pocket as the region into which to dock the selected atoms within the ligand binding site in the NTD. Properly protonated and energy-optimized models of ATP and ADP were then docked with full torsional flexibility in the appropriate (closed or open) semi-rigid receptor pocket model of Hsp80Nc, Hsp82Sc and all substituted versions of both receptors using the 'Dock' application in MOE. The default settings for all of the parameters including Ligand Placement (Triangle Matcher) and Rescoring (London dG) were found to be suitable for reproduction ( $\text{RMSD} < 0.3 \text{ \AA}$ ) of the ligand–receptor complexes as seen in experimentally derived structures. Therefore these settings were used for the rest of the docking simulations, including those involving homology modeling derived receptor structures. The top scoring ligand pose from each docking run was used for calculation of binding energy in the next step. While high-ranking poses other than the top pose were evaluated, they were usually very similar (by both visual examination and RMSD values) to the top pose and equivalent experimentally derived structure.

## 2.4. Calculation of ligand binding energy

The binding energy for top docked ligand poses was calculated with an updated version of a published method [50,51]. Only residues with atoms within  $10 \text{ \AA}$  of the ligand were considered during energy calculations. The overall procedure involves calculating the energies of the docked receptor–ligand complex ( $E_{\text{cpx}}$ ), the unbound ligand in solution ( $E_{\text{lig}}$ ) and the unbound solvated rigid receptor from the complex ( $E_{\text{prot}}$ ) for use in the equation:  $E_{\text{bind}} = E_{\text{cpx}} - (E_{\text{lig}} + E_{\text{prot}})$ . The code and pseudo-code for this procedure is available upon request. For purposes of speed and maintenance of the docked ligand pose, initial optimization in the field of the semi-rigid (fixed heteroatoms) receptor was carried out assuming distance dependent dielectric conditions. Only the final energy calculation step was performed under conditions of solvation and a regime of alternate ligand–receptor flexibility. It should be reiterated that all of the calculated binding energies must be viewed as approximations at different levels of accuracy to the true binding energy. We are aware that the semi-rigid receptor approximation, during ligand docking and initial part of the binding energy calculation, tends to underestimate the effects of induced fit, while the flexible receptor approximation in the final step energy calculation process can overestimate it. It is also likely that at the time-scale of the binding event the receptor cavity cannot change extensively and, therefore, the true binding energy should lie somewhere between the rigid and flexible receptor values. Our previous experience has shown that the correlation of calculated binding energies—discerned with this particular method—to experimentally determined ligand affinities, is remarkably consistent across a number of receptor systems.

## 2.5. Circular dichroism spectroscopy

CD spectra of Hsp80Nc were acquired with a JASCO J-715 Spectropolarimeter (UK) equipped with a thermostatted cell holder, using a quartz cuvette of 1-mm path length over a range of temperatures from 25 to  $45^{\circ}\text{C}$  in 20 mM Tris-HCl (pH 7.5). Spectra were collected over the wavelength range 180–260 nm with a 1 nm bandwidth. For each spectrum, ten scans were collected and averaged. The averaged data were then corrected for background using software supplied by the manufacturer. The CD values were expressed using mean residue molar ellipticity (MRE). Quantitative estimation of secondary structure was obtained by using the CONTIN deconvolution algorithm on the CD deconvolution server—Dichroweb [52,53].

## 2.6. Isolation and purification of Hsp80Nc

Full length Hsp80Nc was isolated in its native state from heat-shocked cultures of a wild type strain of *Neurospora crassa*. A nearly homogeneous product was obtained using a purification procedure entailing the following steps: (i) treatment of crude cell extracts with protamine sulfate; (ii) PEG 8000; (iii) fractionation on hydroxyapatite; (iv) hydrophobic chromatography on Sepharose HP; (v) anion-exchange chromatography on Q-Sepharose (detailed in Supporting Information; Fig. S1).

## 3. Results and discussion

### 3.1. Preliminary structural analysis of Hsp90s

The structural characteristics of individual subunits and truncated Hsp90 constructs from a number of prokaryotic and eukaryotic species were briefly analyzed before being considered for use as structural templates to build homology-based models of

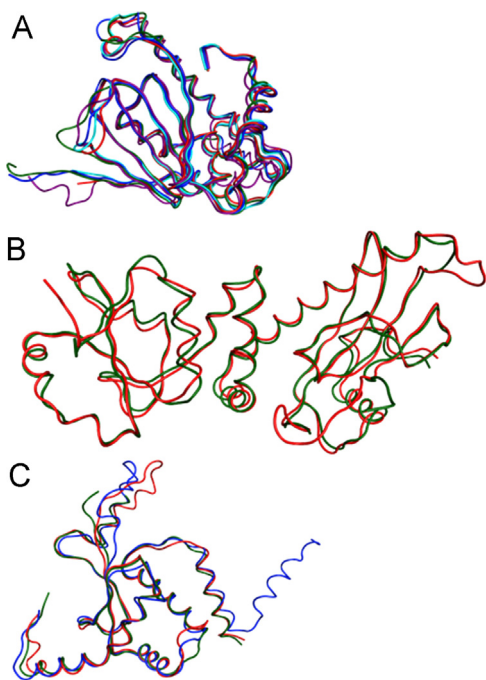


**Fig. 1.** Peptidic backbone overlays of eukaryotic Hsp90 domains. (A) N-Terminal Domains (NTDs): **1amw**: red, **3h80**: green, **2jki**: cyan, **1yt1**: magenta, **2olt**: blue, **1byq**: yellow. RMSD heteroatoms = 2.3 Å, RMSD  $\alpha$ -carbons = 2.1 Å. (B) Middle Domains (MDs): **2cge**: red, **3hjc**: green. RMSD heteroatoms = 1.9 Å, RMSD  $\alpha$ -carbons = 1.8 Å. (C) C-Terminal Domains (CTDs): **2cge**: red, **3hjc**: green, **2olt**: blue, RMSD heteroatoms = 1.8 Å, RMSD  $\alpha$ -carbons = 1.4 Å. (For interpretation of the references to color in this figure legend, the reader is referred to the web version of the article.)

Hsp80Nc. These structures ranged from (i) almost complete proteins, **2iop** and **2ioq** from *Escherichia coli* [54]; (ii) truncated or partial proteins, **2cge** and **2cg9** from *Saccharomyces cerevisiae* [33], **3hjc** from *Leishmania major* and **201t** from *Canis familiaris* [55]; (iii) N-Terminal domains with co-crystallized ligands from *Saccharomyces cerevisiae* (**1amw**) [18], *Leishmania major* (**3h80**), *Hordeum vulgare* (**2jki**) [56], *Canis familiaris* (**1yt1**) [55] and *Homo sapiens* (**1byq**) [57]. We did not use the N-terminal domain from *Plasmodium falciparum* as it exhibits a high degree of structural similarity to its counterparts in the aforementioned eukaryotic species [58]. The results of this analysis, entailing peptidic backbone overlays of the three major domains, partially shown in Fig. 1, attest to the high level of overall structural homology for these domains in species as diverse as *S. cerevisiae* and *H. sapiens*.

The RMSD (Root Mean Square Deviation) values for aligned and optimally overlapped heteroatoms of the same domain from various eukaryotic species range from 2.3 Å for the NTDs to 1.8 Å for the CTDs. The very high degree of structural homology in conjunction with >60% sequence homology (Supporting Information Fig. S2) suggests that the basic mechanisms underlying the functioning and co-chaperone interaction patterns of Hsp90s are conserved across a wide range of eukaryotic species.

Within the largely rigid NTD, two mobile regions are intimately involved in the concurrent processes of ATP binding and dimerization: (i) the first 22–23 residues in the N-terminal region and (ii) the ‘lid’ region constituting residue 93–124 in Hsp80Nc and 91–122 in Hsp82Sc. Our current understanding of the mobility of, and interplay between, these regions in the NTD is based on investigation of the known structural changes between the inactive ADP-bound (**1amw**) form of Hsp82Sc and its active ATP-bound (**2cg9**) form [18,33]. The structural changes known to occur during activation as highlighted in Fig. 2, show both states of the NTD [59–61]. The ‘lid’ of the inactive form of the NTD is curled back and

held in a predominantly helical conformation, thereby exposing part of the ligand-binding pocket (Fig. 2A). Activation and subsequent dimerization of Hsp82Sc appear to release the ‘lid’ region enabling it to interact with residues lining the ligand-binding site thus enclosing the bound nucleotide (Fig. 2B). For reasons that are still incompletely understood, release of the ‘lid’ is linked to an almost simultaneous change in the position and structure of the N-terminal ~20 residues of the NTD. The N-terminal region of the NTD changes from a  $\beta$  strand in an intra-domain interaction (Fig. 2A), to the extended coil-like conformation (Fig. 2B) which is stabilized by interaction with complementary residues in the NTD of the opposite chain in the dimer (not shown). It is generally accepted that activating co-chaperones, in addition to enhancing dimer formation, somehow facilitate structural changes that favor the active ATP-bound state of the NTD.

### 3.2. Validation of homology modeling methodology

The first step in building homology-based models of Hsp80Nc and Hsp82Sc involved validating the methods and tools to be used in their construction. A more detailed account is provided in the Homology Modeling Procedure subsection of the Experimental Section. Two aspects of the homology modeling procedure were tested; (i) the ability to consistently place residue side-chains in positions and conformations similar to those seen in X-ray crystallographic models of the protein; (ii) the ability to generate high-quality models of a protein from a structural template with 60–70% residue homology.

The first validation exercise utilized **1amw** as both the target sequence and structural template [18]. We wished to determine if the energy minimization routines used in our homology modeling procedure resulted in the placement of residue side-chains in a manner consistent with that seen in X-ray crystallography derived models of **1amw**. As shown in Fig. 3A–C, our homology-modeling procedure created a model of **1amw** with a high level of structural similarity to its experimentally derived structure, exhibiting an almost identical placement of side chains lining the ligand-binding-site. The quality of the homology-based model of **1amw** was evaluated by multiple methods built into MOE 2008.10, and found to be almost identical to its experimentally derived structure [62].

The second validation exercise used **1amw** as the target sequence and **1byq** as the structural template. The level of sequence homology between them (65–70%) is comparable to that between equivalent domains of Hsp80Nc and Hsp82Sc. As also shown in Fig. 3D–F, our modeling procedure generates a model of **1amw** with a high degree of similarity to its experimentally derived structure. The quality of residue side chain placement was also consistently good. It, therefore, appeared that our homology modeling methodology was capable of creating high quality homology-based models of isolated domains from Hsp90s, under conditions where the sequence homology between the target and template exceeded 60%. Representative results for evaluations of the model quality are presented in Supporting Information Fig. S3. We further validated our methodology by creating homology-based models of the Hsp82Sc MD from **2cge** based on the one found in **3hjc** and the Hsp82Sc CTD domain from **2cg9** based on the corresponding one in **201t**. In all instances, the homology-based models were very similar to the experimentally derived models of the same as defined by RMSD values <1 Å for heteroatoms. Moreover, they were comparable to experimentally derived models of the same protein based on results of multiple methods used to evaluate the quality of such models (not shown) [62]. Previously published studies have shown that high quality homology-based models can be used as substitutes for experimentally determined structures in ligand-docking experiments [63–65]. The quality of

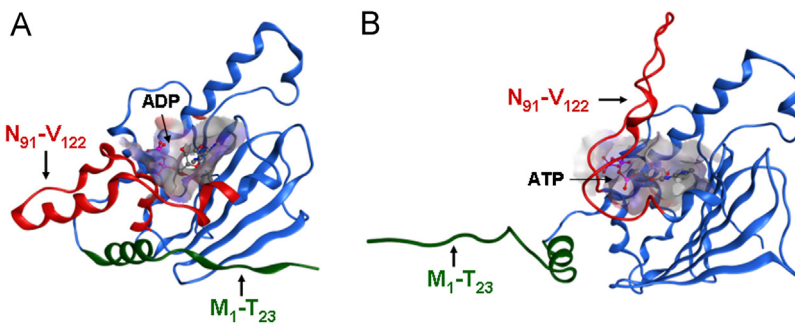


**Fig. 2.** Activation-induced structural changes in the NTD of Hsp82Sc. (A) The inactive ADP-bound form and (B) the active form of Hsp82Sc NTD. The mobile 'lid' region: red and N-terminal region: green are highlighted to illustrate changes in their secondary structure and position relative to the rest of the NTD: blue. (For interpretation of the references to color in this figure legend, the reader is referred to the web version of the article.)

homology-based models was, therefore, especially important since we intended to use them in calculations of the approximate binding energy of physiological ligands (ATP and ADP) when docked into the primary active site of Hsp80Nc and Hsp82Sc.

### 3.3. Modeling the major domains of Hsp80Nc and Hsp82Sc

A number of homology-based models of the NTD in Hsp80Nc, based upon the experimentally derived structures of the same domain from other Hsp90s, were created and compared with each other. These models (Fig. 4A and B) were very similar, even though they were based upon structural templates from a range of eukaryotic species. Their quality was also evaluated and found to be satisfactory and comparable to their parent structures (not shown). We selected the **1amw**-based model as the representative version of an 'open lid' (inactive) form of Hsp80Nc NTD for subsequent reconstructions of the Hsp80Nc monomer, since its structural template displayed the highest degree of sequence homology to the target sequence. The 'closed lid', and therefore active, form of the Hsp80Nc NTD (not shown in Fig. 4) was modeled on the equivalent domain in **2cg9** and used for subsequent reconstruction of Hsp80Nc dimer.

While experimentally derived structures from three eukaryotic species (*S. cerevisiae*, *L. major* and *C. familiaris*) were available as structural templates for modeling the MD, we opted to use only the first two since the third one (Grp94 from *C. familiaris*) is an Hsp90 isoform specific to the endoplasmic reticulum. Models of the Hsp80Nc MD, based on both structural templates, are also

shown in Fig. 4C and D. In all subsequent reconstruction of full-length Hsp80Nc monomers and dimers we chose the **2cge**-based model of the MD, because it exhibits the highest sequence homology to Hsp80Nc. A structural analysis of the Hsp80Nc MD model and comparison with its structural template (the MD in **2cge**) is shown in Supporting Information Figure S4. Three experimentally derived structures of the CTD of Hsp90s (*S. cerevisiae*, *L. major* and *C. familiaris*) were used as structural templates for models of that domain in Hsp80Nc, as depicted in Fig. 4E and F. Once again, the **2cge**-based model was selected for subsequent reconstructions of Hsp80Nc monomer and dimer models, as it exhibited the highest degree of sequence homology to the target sequence. A structural analysis of the Hsp80Nc CTD model along with a comparison with its structural template (the CTD in **2cge**) is shown in Supporting Information Fig. S5.

As stated in the Introduction, a full-length experimentally derived structure of Hsp82Sc is still not available even though a large number of structures for its major domains and truncated constructs, such as **2cg9**, can be readily found in the literature. Therefore, we decided to construct full length models of Hsp82Sc monomer and dimer using the same methodology and tools employed for Hsp80Nc. Homology modeling to recreate readily available molecular structures might appear unconventional, but doing so allowed us to perform energy minimization and placement of residue side-chains under molecular force-field conditions identical to those used for Hsp80Nc. Models of the three major domains of Hsp82Sc were created based on the following structural templates: **1amw** ('open lid' NTD), **2cg9** ('closed lid' NTD), **2cge** (MD)

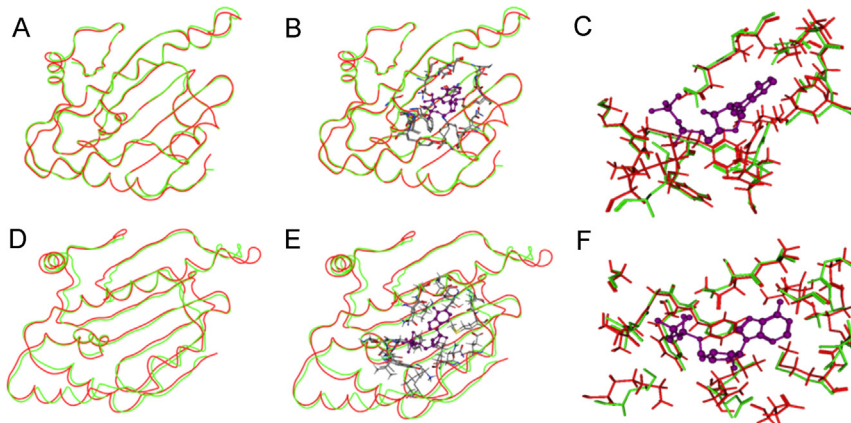


**Fig. 3.** Comparison of homology-based models of the NTD from Hsp82Sc with its experimentally derived structure. (A) and (B) The peptidic backbones of the **1amw**-based homology model of **1amw**: red and **1amw**: green; RMSD heteroatoms = 0.7 Å. Residues around the ligand, ADP, are shown in (B) and (C); RMSD heteroatoms in the ligand-binding site = 0.6 Å. (D) and (E) The peptidic backbones of the **1byq**-based model of **1amw**: red and **1amw**: green; RMSD heteroatoms = 1.2 Å. Residues around ADP are shown in (E) and (F); RMSD heteroatoms in the ligand-binding site = 0.7 Å. (For interpretation of the references to color in this figure legend, the reader is referred to the web version of the article.)

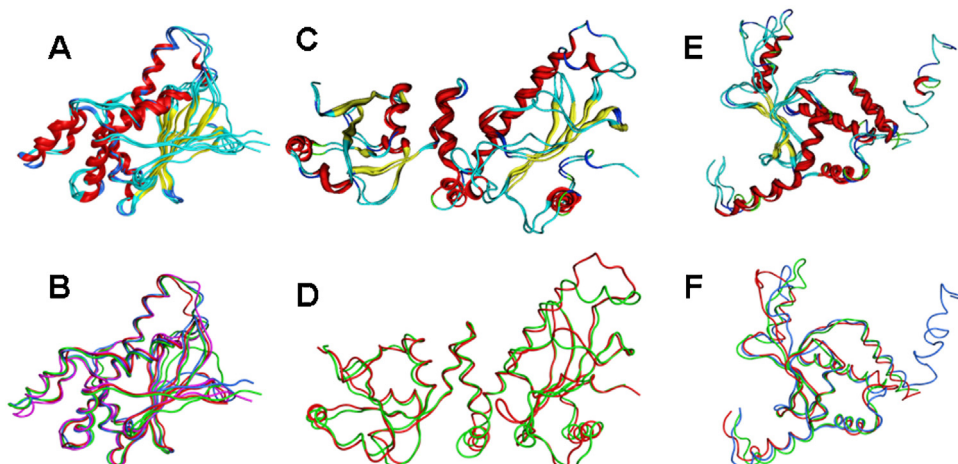


**Fig. 4.** Overlaid homology-based models of Hsp80Nc NTD, MD and CTD. Two representations of NTD models based on **1amw**, **3h80**, **2jki**, and **1byq** are shown in (A) and (B). In (B): **1amw**: red, **3h80**: green, **2jki**: blue, and **1byq**: magenta; RMSD heteroatoms = 1.6 Å. Two representations of MD models based on **2cge** and **3hjc** are shown in (C) and (D). In (D): **2cge**: red and **3hjc**: green; RMSD heteroatoms = 1.6 Å. Two representations of CTD models based on **2cge**, **3hjc** and **2olt** are shown in (E) and (F). In (F): **2cge**: red, **3h80**: green and **2olt**: blue; RMSD heteroatoms = 1.7 Å. (For interpretation of the references to color in this figure legend, the reader is referred to the web version of the article.)

and **2cge** (CTD). Models of the major Hsp82Sc domains also underwent, and passed, multiple evaluations of quality identical to those previously described for Hsp80Nc (not shown).

#### 3.4. Modeling the 'charged' linker in Hsp80Nc and Hsp82Sc

The aligned sequences of the 'charged' linker region in eukaryotic Hsp90s contain alternating stretches of positive and negatively charged residues (Fig. 5A). The degree of cross-species sequence homology for this region is lower than that witnessed in the major domains; however, the overall pattern of residue arrangement is remarkably consistent across species. While the 'charged' linker is conventionally assigned a collapsed coil structure, a hairpin structure with significant  $\beta$  strand content is also plausible primarily because of the alternating bands of highly charged residues. The results of cryo-electron microscopy imaging suggest that this region is partially flexible, and deletion studies indicate that the 'charged' linker contains the attachment sites of some co-chaperones [34,43,66]. We attempted to address this issue by measuring the CD spectra of Hsp80Nc under conditions where robust ATPase activity had been demonstrated.

The secondary structure content of Hsp80Nc, as determined by diverse CD deconvolution algorithms is shown in Table 1 [67]. Deconvolution of the CD spectra of Hsp80Nc using multiple algorithms consistently reported a  $\beta$  strand content of over 30% and an  $\alpha$  helical content not exceeding 30%. An analysis of the three major domains of Hsp82Sc (Table 2) suggests a higher percentage of helical content (>40%) and a lower  $\beta$  strand content (<20%). As previously stated, the three major domains of Hsp82Sc, accounting for ~90% of the residue count, display a high level of sequence homology to equivalent domains in Hsp80Nc. Furthermore, as shown in Fig. 1, the major domains of Hsp90s have markedly similar secondary and tertiary structures across a wide range of eukaryotic (and prokaryotic) species. It is, therefore, reasonable to assume

that secondary structure of residues comprising the three major domains of Hsp80Nc (610–615 out of the 700 odd residues) is, for all practical purposes, identical to that of the corresponding domains in Hsp82Sc. While dimer formation is expected to result in some structural changes in the major domains, the number of residues in the relevant regions does not exceed 3–4% of the total. Therefore residues in the 'charged' linker and the C-terminal tail, which are always omitted from constructs used in X-ray crystallography, had to account for the majority of differences observed between the secondary structure content as determined by CD spectra versus that derived from a sum of the experimentally determined domain models.

The discrepancy between the secondary structure content of full-length Hsp80Nc, as determined by CD spectroscopy, and the sum of the major domains from the structurally almost identical Hsp82Sc is best reconciled if a significant percentage of residues in the uncharacterized regions were to attain a  $\beta$  strand-type secondary structure. We, therefore, propose that while the 'charged' linker has significant  $\beta$  strand content, it is largely in the form of loose associations of  $\beta$  strands, as opposed to the conventional well-defined and rigid  $\beta$  sheets. The peptide builder module in MOE was used to construct a model of the 'charged' linker in Hsp80Nc. Alternating strands of charged residues were modeled as  $\beta$  strands, with intervening regions being modeled as random coils. The scheme used for the assignment of secondary structure to residues in the linker region of Hsp80Nc is depicted in Fig. 5B. The charged regions in the linker were then positioned such that those with opposing charges could interact with each other in a manner similar, but not identical, to  $\beta$  sheets. A preliminary model of the 'charged' linker is shown in Fig. 6A. An almost identical procedure was used for creating a model of the 'charged' linker region in Hsp82Sc (not shown). The positioning and linkage pattern of the charged segments is such

**Table 1**

CD Spectra deconvolution of full-length Hsp80Nc using various algorithms with DichroWeb [67].

Method	Helical Content	$\beta$ Strand Content	Random Coil	NRMSD
SELCON3	0.223 (22%)	0.333 (33%)	0.348 (35%)	0.098
CONTIN	0.301 (30%)	0.326 (33%)	0.372 (37%)	0.039
CDSSTR	0.200 (20%)	0.370 (37%)	0.420 (42%)	0.030

**Table 2**

Secondary Structure Content of the experimentally validated models for Major Domains in Hsp82Sc (as measured by MOE 2008.10).

Domain	% Helical ( $\alpha + 3-10 + \pi$ )	% $\beta$ strand	% Random Coil
NTD	49	21	33
MD	47	16	37
CTD	62	9	29
<b>Sum</b>	<b>46</b>	<b>16</b>	<b>32</b>



**Fig. 5.** Aligned residue sequences of the 'charged' linker region in various eukaryotic Hsp90s. The presence of alternating bands of acidic: red and basic: blue residues, as well as the species-specific differences in the length of this region are evident in (A). Assignment of secondary structure for residues in the 'charged' linker of Hsp80Nc is shown in (B): R: random coil; S:  $\beta$  strand; T: turn. Hsp80Nc (*Neurospora crassa*); Hsp82Sc (*Saccharomyces cerevisiae*); Hsp90Lm (*Leishmania major*); Hsp90Hv (*Hordeum vulgare*); Hsp90Hs (*Homo sapiens*).

that it allows for orderly extension, and compaction, of the 'charged' linker region as seen in Fig. 6A and B, respectively. Co-chaperones binding to the 'charged' linker could readily perturb the balance of interactions which favor the compacted form and thus unwind it. Conversely, the lack of co-chaperones, or their displacement by adjacent co-chaperones, would tend to favor transformation of the extended form to its compacted form.

### 3.5. Modeling the 'C-terminal tail' in Hsp80Nc and Hsp82Sc

The final 35-odd, species-specific residues of the CTD, were also reconstructed for both proteins since they are not found in available experimentally derived structures of Hsp90s. This C-terminal tail region was, in contrast to the 'charged' linker, reconstructed as a random coil as it lacked sequence features strongly associated with any particular secondary structure. Moreover, as the C-terminal end segment is known to interact with many co-chaperones it is likely to be fairly flexible. Both of the above described models—the charged linker and the C-terminal end—were incorporated into reconstructions of full-length Hsp80Nc and Hsp82Sc. The procedure and process of reconstructing these proteins, as monomers and dimers, is described in the following.

### 3.6. Reconstruction of 'extended' Hsp80Nc and Hsp82Sc monomers

An 'extended' version of the Hsp80Nc monomer model was assembled on a template based on the *E.coli* Hsp90 ortholog, HtpG (**2iop**), as it was the most complete experimentally derived model of a non-truncated 'open' monomer form for Hsp90s albeit from a prokaryote [54]. Our choice of the **2iop** template should not

be construed as rejection of alternative structures for Hsp80Nc and Hsp82Sc monomers. The documented conformational flexibility of Hsp80Sc does allow for multiple structural versions of Hsp90 monomers and many such structural arrangements have been observed in cryo-electron microscopy based studies of Hsp90s [40]. Our **2iop**-based models of the Hsp80Nc and Hsp82Sc should, therefore, be viewed as the most common, or likely, monomeric form of these two proteins.

The process of Hsp80Nc monomer reconstruction commenced with the superimposition of previously constructed models of its major domains on the chosen template. Each major domain was carefully aligned and superimposed on the template as illustrated in Fig. 7A. The short linker between the C-terminus of the Middle Domain (MD) and N-terminus of the C-Terminal domain (CTD) was reconstructed as a random coil using the peptide builder module in MOE 2008.10. The next step involved importing, placing and splicing the afore-mentioned 'charged' linker into the reconstruction. Finally, the C-terminal model was imported and spliced into its proper position. The reconstructed, and now complete, model of the Hsp80Nc monomer was subjected to a process of structural optimization via alternating rounds of energy minimization and molecular dynamics wherein the position of the major domains was constrained. The structural optimization of the newly inserted flexible linkers was stopped once they settled into a stable structure with a consistent pattern of residue interaction with surrounding domains (Fig. 7B). The results of evaluations of the quality of the Hsp80Nc 'extended' monomer model are shown in Supporting Information Fig. S6. The overall procedure for reconstructing the Hsp82Sc monomer model (not shown) was identical to that described for the Hsp80Nc monomer, except for the identity of the domain and linker models used in its creation.

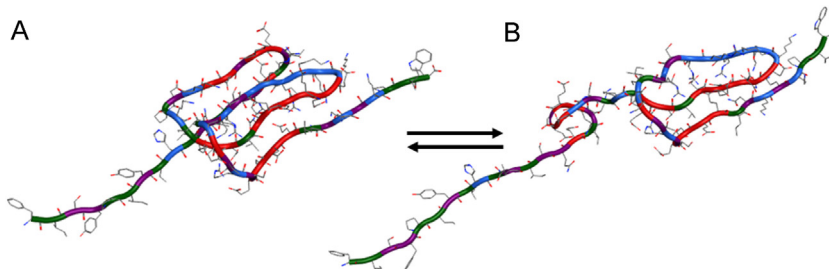


**Fig. 6.** Models depicting primary reconstructed structures for the 'charged' linker in Hsp80Nc. (A) are a simplified schematic depiction of the proposed compacted  $\beta$ -strand rich form of the linker. The partially extended post-activation form, depicted in (B), exposes residues in the core of the linker to the external environment thereby facilitating potential interaction with co-chaperones.

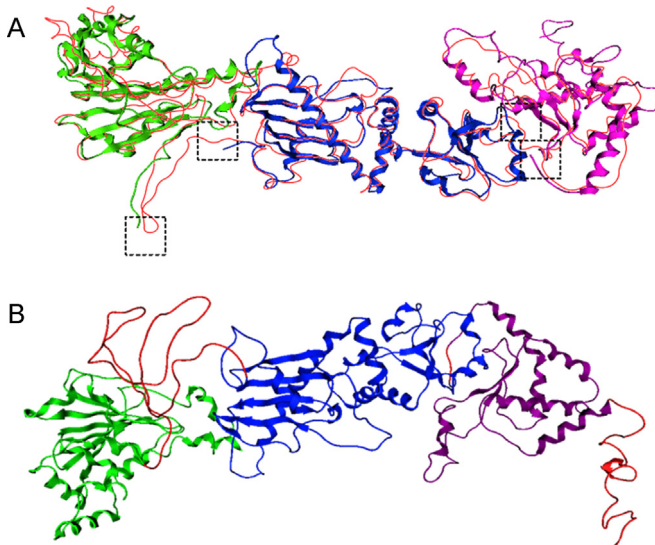


**Fig. 7.** Reconstruction of the **2iop**-based Hsp80Nc ‘open’ monomer. The peptidic backbone template of **2iop** is rendered as a thin red line in (A). Reconstructed linkers were subsequently spliced in at the points highlighted with dashed boxes in (A). The final and optimized model of the ‘open’ Hsp80Nc monomer with reconstructed and optimized linker is shown in (B); NTD: green, MD: blue, CTD: purple and linkers: red.

### 3.7. Reconstruction and reconstitution of Hsp80Nc and Hsp82Sc apo-dimers

The overall methodology for reconstructing models of the Hsp80Nc and Hsp82Sc dimer was similar to that used for creating the monomer models. The Hsp82Sc dimer construct in **2cg9** was used as the structural template for assembly of the complete dimer models. Although the template was a truncated version of the Hsp82Sc dimer, it was sufficiently complete for use as a starting point for the reconstruction. Each of the two chains constituting the dimer, henceforth referred to as ‘half-dimer’, was individually reconstructed before reconstitution as the dimer. The first ‘half-dimer’ of the Hsp80Nc model (chain A) was assembled on a template based on the equivalent chain in **2cg9**. Each major domain was carefully aligned and superimposed with its equivalent on the template structure. The short linker between the C-terminus of the Middle Domain (MD) and N-terminus of the C-Terminal domain (CTD) was reconstructed as a random coil using the peptide builder module in MOE. The ‘charged’ linker model was then imported, placed and spliced into the ‘half-dimer’. The C-terminal model was the last piece to be imported and spliced into the ‘half-dimer’ model. The reconstructed model (chain A) was, once again, subjected to alternating rounds of energy minimization and molecular dynamics in which the position of the major domains was constrained. The process of structural optimization was continued until the flexible linkers settled into a stable conformation and consistent pattern of residue interaction with surrounding domains. The resultant ‘half-dimer’ model is depicted in Fig. 8A. The other chain of the Hsp80Nc dimer, as well as both chains of the full-length Hsp82Sc dimer, was also reconstructed employing a similar procedure.

Structural models of both Hsp80Nc ‘half-dimers’ (chain A and B) were then combined to create a preliminary model of the apo-dimer. The Cartesian coordinates of most residues in the apo-dimer model were almost identical to their counterparts in the **2cg9** template, and hence did not require further structural optimization. However, some residues near the contact surfaces of major domains did exhibit a moderate degree of steric clash, necessitating further structural optimization. This was achieved by performing a series of short molecular dynamics-based energy optimizations on

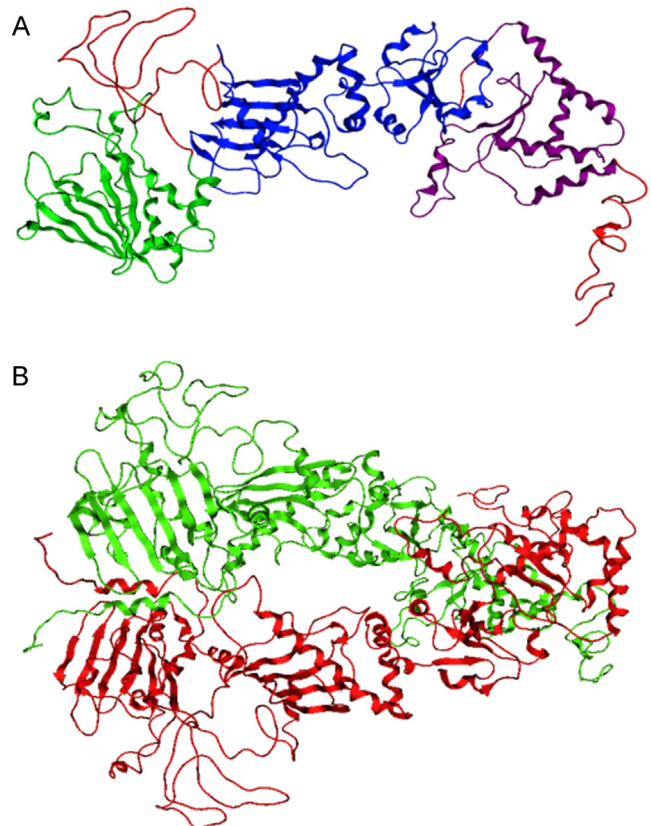


**Fig. 8.** Optimized models of the Hsp80Nc ‘half-dimer’ and dimer. The major domains in the ‘half dimer’ model depicted in (A) are: NTD: green, MD: blue and CTD: purple. Linkers and reconstructed sections are colored red. Optimized Hsp80Nc dimer model showing both ‘half-dimers’ is shown in (B): chain A: red and chain B: green. (For interpretation of the references to color in this figure legend, the reader is referred to the web version of the article.)

residues within 4.5 Å of the inter-chain contact surface. The procedure removed adverse vdW contacts between interacting residues, in addition to optimizing hydrogen bond formation between the two chains. The resultant model (Fig. 8B) retains considerable overall resemblance to the template (**2cg9**) used to assemble it. However, unlike its template, the Hsp80Nc model is neither truncated nor constrained by fragments of the co-chaperone (Aha1). The same procedure was used to reconstruct the Hsp82Sc apo-dimer with the corresponding set of ‘half-dimer’ chains. Partial structural analysis of the Hsp80Nc apo-dimer model, as shown in Supporting Information Fig. S7 indicates that it is equivalent in quality to the experimentally derived structural template used for its assembly. Analysis of the non-truncated Hsp82Sc apo-dimer model yielded similar results (not shown).

### 3.8. Inter-chain residue contacts in the Hsp80Nc apo-dimer models

The two constituent chains in the Hsp80Nc apo-dimer model (Fig. 9) appear to have extensive surface interactions between them. The two truncated Hsp82Sc chains in the structural template (**2cg9**) used to create the Hsp80Nc apo-dimer model also exhibit similar and extensive inter-chain interactions. Interestingly, the energy and structural minimization procedures used to optimize the interactions of residues near the interface of the two chains, in the Hsp80Nc model, seem to unmask interactions not evident in the structural template. The majority of residues participating in inter-chain interactions in the Hsp80Nc apo-dimer model are either charged (Lys, Arg, Glu, Asp) or hydrophilic (Asn, Gln, Thr,

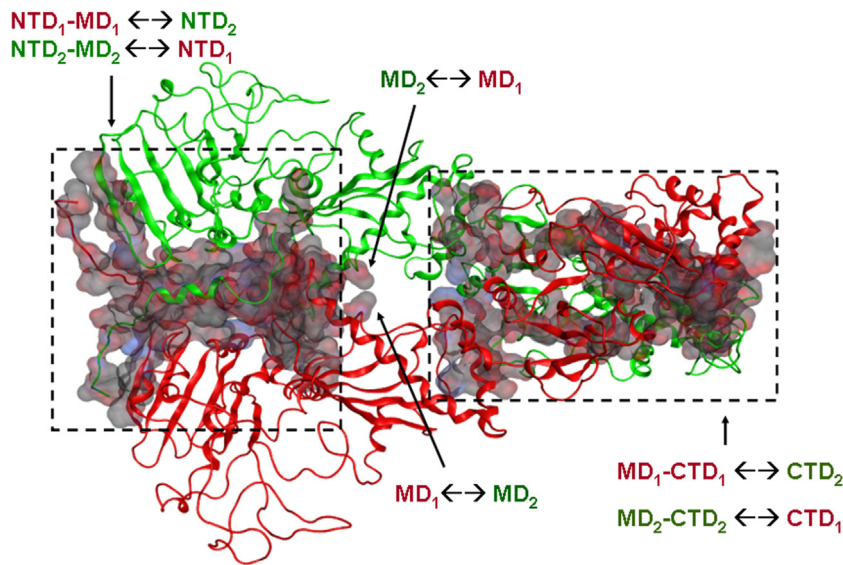


**Fig. 9.** Inter-chain interaction surface in the reconstructed Hsp80Nc dimer. The Hydrophilic surface interactions are rendered as red or blue while the hydrophobic ones are shown in grey. The majority of inter-chain interactions occur between (i) NTD and MD of one chain with the NTD in the other and vice versa; (ii) the MD-CTD from one chain with the CTD from the other and vice versa. (For interpretation of the references to color in this figure legend, the reader is referred to the web version of the article.)

Ser). Therefore, inter-chain hydrogen bonds would form the bulk of interactions between the two monomers in the Hsp80Nc (and Hsp82Sc) apo-dimer. The lack of significant hydrophobic interactions, to bolster the extensive hydrophilic contacts between the two chains, might also explain why Hsp90 dimers seemingly dissociate as readily as they form. The next few sections examine the interactions of the three major domains in one chain of the Hsp80Nc dimer with their counterparts in the other chain.

### 3.9. Residue contacts and interactions of the NTDs in the Hsp80Nc apo-dimer

The NTDs in the homology based apo-dimer of Hsp80Nc, predictably, make contacts similar to those observed in the equivalent region of its structural template, **2cg9**. As shown in Fig. 10, the observed interactions involve: (i) The N-terminal region of one chain and its complementary sequence in the other, and vice versa; (ii) Residues from the N-terminal region of one NTD with those near the ‘lid’ of the other. The first set of interactions, between the N-terminal end of one NTD ( $M_1$ ATAET<sub>6</sub>) and a complementary region in other NTD ( $G_{157}$ TFTIRP<sub>163</sub>), were similar to those seen in the structural template, **2cg9**. The second set of interactions, between the remainder of the first 20-odd residues in the N-terminal end of one NTD ( $E_8$ FQAEISQLLSLIINT<sub>23</sub>) and residues that were close to ( $F_{123}$ GV<sub>125</sub>), or part of ( $G_{97}$ TIAR<sub>101</sub>), the ‘lid’ region of the other NTD could represent a potential mechanical linkage between the formation of dimers and stabilization of the closed ‘lid’ in the NTD.

### 3.10. Residue contacts and interactions of the MD in the Hsp80Nc apo-dimer

The majority of inter-chain interactions of the MD are with the NTD and CTD from the other chain (Fig. 11A). While interactions of the MD in one chain with its counterpart in the other do occur, they are sparse as previously shown in Fig. 9. The first significant inter-chain interactions involve a stretch of residues in the MD ( $P_{360}$ LNLSRETQQNKI<sub>373</sub>) with another from the NTD ( $N_{22}$ TVYSNKEI<sub>30</sub>) of the other chain (Fig. 11B). As noted in the previous section, and shown in Fig. 10B, residues  $N_{22}$  and  $T_{23}$  are also involved in interactions that stabilize the active form of the NTD. It therefore appears that the MD within an Hsp80Nc

dimer can indirectly stabilize the active (ATP-bound) form of the NTD in its own chain, via a direct interaction with the NTD in the other chain and vice versa. The second set of major inter-chain interactions of the MD are with the CTD of the other chain. The first such interaction, shown in Fig. 11C, between  $S_{404}$ AFSK<sub>408</sub>,  $E_{462}$ SIKAVSK<sub>469</sub> and  $D_{488}$ PIDEY<sub>493</sub> from one chain with  $K_{580}$ AQALR<sub>585</sub> and  $T_{643}$ IDEPASLP<sub>651</sub> from the other is rather straightforward and similar to that seen in **2cg9**. The second and novel interaction ( $K_{477}$ EK<sub>479</sub> with  $E_{685}$ TGDSAMEEV<sub>695</sub>) involves the MD and the reconstructed C-terminal end of the CTD (Fig. 11C).

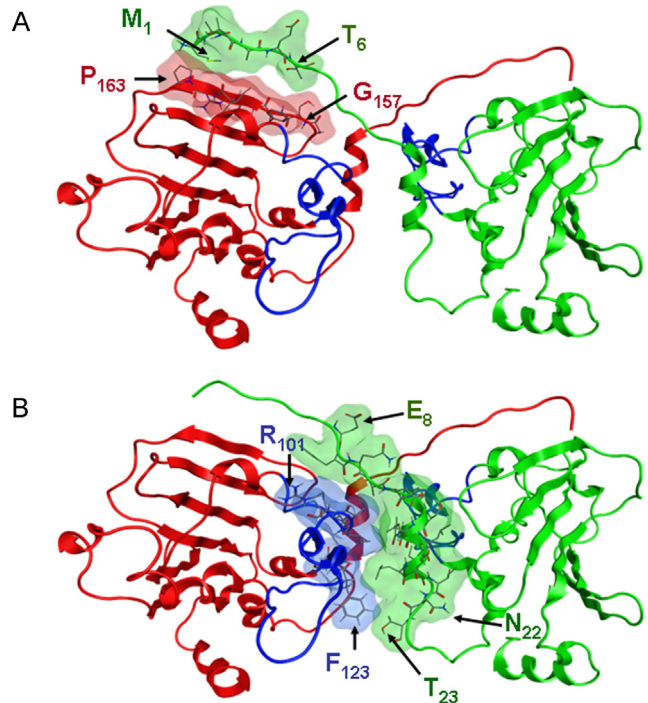


**Fig. 10.** Inter-chain interactions between NTDs in the Hsp80Nc apo-dimer model. The major inter-chain interactions occur between the following epitopes: (A)  $M_1$ ATAET<sub>6</sub> with  $G_{157}$ TFTIRP<sub>163</sub> and (B)  $E_8$ FQAEISQLLSLIINT<sub>23</sub> with  $G_{97}$ TIAR<sub>101</sub> and  $F_{123}$ GV<sub>125</sub>.

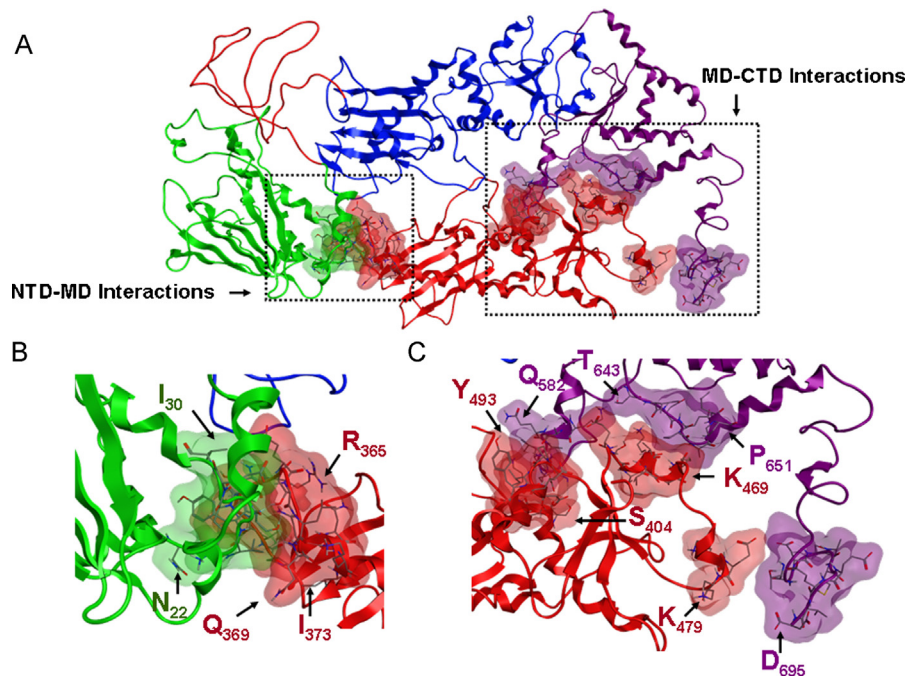


**Fig. 11.** Inter-chain interactions of the MD in the Hsp80Nc apo-dimer model. (A) An overview of the major interactions between the MD from chain A (MD-A) and all three domains of chain B; NTD-B: green, MD-B: blue and CTD-B: magenta. (B) The first of the two major classes of interactions occur between  $P_{360}$ LNLSRETLQQNKI $_{373}$  and  $N_{22}$ TVYSNKEI $_{30}$  from MD-A and NTD-B respectively. (C) The second major class of interactions occur between  $S_{404}$ AFSK $_{408}$ ,  $E_{462}$ SIKAVSK $_{469}$  and  $D_{488}$ PIDEY $_{493}$  from MD-A and  $K_{580}$ AQALR $_{585}$  and  $T_{643}$ IDEPASLP $_{651}$  from CTD-B. A minor, but important, interaction between  $K_{477}$ EK $_{479}$  to  $E_{685}$ TGDSAMEEVED $_{695}$  is also shown in (C). (For interpretation of the references to color in this figure legend, the reader is referred to the web version of the article.)

### 3.11. Residue contacts and interactions in the CTD of the Hsp80Nc apo-dimer

The majority of inter-chain residue contacts for the CTD occur with the MD and CTD from the other chain of the dimer. Interactions between the CTD from one chain and MD from the other one have been described in the preceding section (Fig. 11C). The major inter-chain interactions between the two CTDs, are similar to those observed in the **2cg9** complex, and comprise mutual interactions between two epitopes, namely  $P_{606}$ IIKELKKKVETD $_{618}$  and  $T_{643}$ IDEPASLPRGIHKLVSLGQ $_{662}$  (Fig. 12).

### 3.12. Multi-domain interactions in the Hsp80Nc apo-dimer

One of the intriguing and novel features of the full-length models of Hsp80Nc concerns the oddly symmetrical nature of multi-domain interactions. There are apparently two pairs of such interactions; for visual clarity only one example of each type is shown in Fig. 13A. The first one involves  $P_{360}$ -I $_{373}$  from the MD of chain A with part of the N-terminus ( $E_8$ -T $_{23}$ ) from the NTD of Chain B, which in turn interacts with two epitopes (G $_{97}$ -R $_{101}$  and G $_{123}$ -V $_{125}$ ) in the 'lid' region of the NTD from Chain A (Fig. 13B). It is plausible that this complex interaction could be complicit in stabilization of the nearby ligand-binding cavity in the 'closed lid' dimeric version of Hsp80Nc. A similar multi-domain interaction at the other end of the dimer model involves K $_{477}$ -K $_{479}$  from the MD and E $_{516}$ -K $_{523}$  of the CTD of chain A with E $_{685}$ -D $_{695}$  from the CTD of chain B and vice versa. It is noteworthy that K $_{523}$  from Hsp80Nc is the analogue (by sequence alignment) of K $_{560}$  from Human Hsp90 $\alpha$ , which has been shown to interact with Novobiocin—a known inhibitor of the incompletely characterized nucleoside binding site in the CTD of Hsp90s [68]. The first multi-domain interaction (Fig. 13B) is also witnessed, albeit to a lesser extent, in the experimentally obtained **2cg9** structure. However, the second type of interaction (Fig. 13C) is novel since

experimentally derived structures of Hsp90s lack the last 35 residues in the C-terminal domain, containing the residues in Hsp80Nc (E $_{685}$ -D $_{695}$ ) involved in this interaction. It is noteworthy that the second multi-domain interaction is similar to the first one, in that both use terminal residues from a domain in the other chain to stabilize an intra-chain interaction between two adjacent domains. Furthermore, the first multi-domain interaction potentially stabilizes the ligand-binding pocket in the NTDs of the dimer, and the second one is adjacent to a residue (K $_{523}$ ) involved in binding to a known ligand of the nucleoside-binding site in the CTD [68].

### 3.13. Overall dimensions and shape of the Hsp80Nc 'apo-dimer' model

As stated in the Introduction, monomers, dimers and larger complexes of various Hsp90s have been imaged using cryo-electron microscopy [34]. While these images have insufficient resolution to yield much information about the detailed structure of Hsp90s, they have been invaluable in following changes in the overall shape and relative positions of its subunits. The overall dimensions, shape and surface characteristics of our homology based models of Hsp80Nc (Supporting Information Fig. S8) show considerable similarity to the twisted donut shape of other eukaryotic Hsp90 dimers, as revealed by electron microscopy based techniques [69,70]. The remainder of this section is devoted to a study of the interactions of physiological ligands of Hsp90s with X-ray crystal structure and homology based models of Hsp82Sc and Hsp80Nc NTD, with the objective of understanding the reasons underlying the higher basal ATPase activity of Hsp80Nc.

### 3.14. Binding energies of physiological ligands

The rationale for using the NTD, as opposed to the whole protein, for calculating the binding energy of physiological Hsp90s ligands

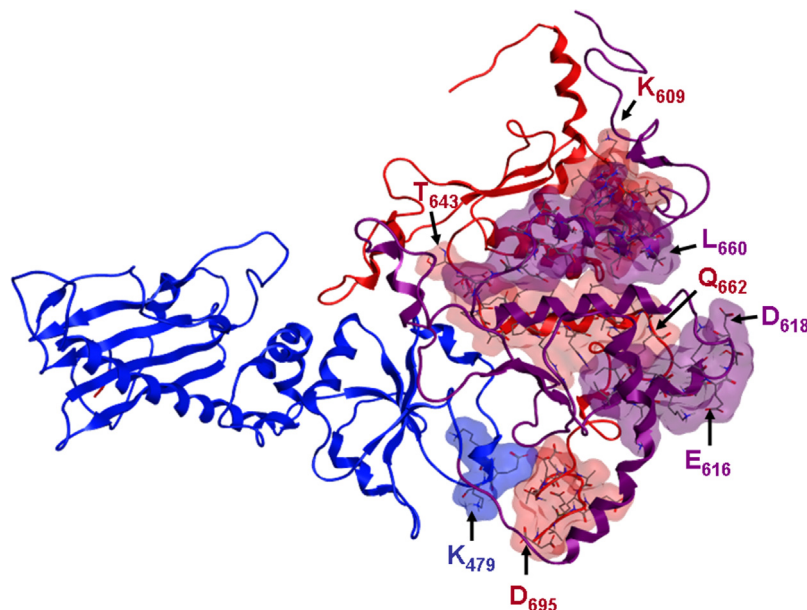


**Fig. 12.** Inter-chain interactions between the CTDs in the Hsp80Nc apo-dimer model. Most interactions occur between P<sub>606</sub>IILKEKKVETD<sub>618</sub> in one chain with T<sub>643</sub>IIDEPAASLPRGIHKLVSLGQ<sub>662</sub> from the other and vice versa. Interactions between E<sub>685</sub>TGDSAMEEV<sub>D695</sub> in the CTD of one chain with K<sub>477</sub>EK<sub>479</sub> in the MD of the other one, previously depicted in Fig. 11(C), are also shown.

(ADP/ATP) is based on the following observations: (1) Molecular mechanics based calculations of ligand-binding energies are insensitive to the presence or absence of residues farther than 5–7 Å from the ligand-binding cavity—the NTD in Hsp80Nc (and Hsp82Sc) contains all residues up to 10 Å from the cavity; (2) Most ligand-docking protocols, including the ones implemented in MOE 2008.10, are

also insensitive to the residues beyond 5–7 Å of the ligand-binding pocket surface. Moreover, an experimentally derived structure of monomeric, and ADP- or ATP-bound, full-length Hsp82Sc (replete with its charged linker and C-terminal tail) is not available.

Admittedly, ligand-binding energies, calculated by methods based in molecular mechanics tend to have high relative, but low

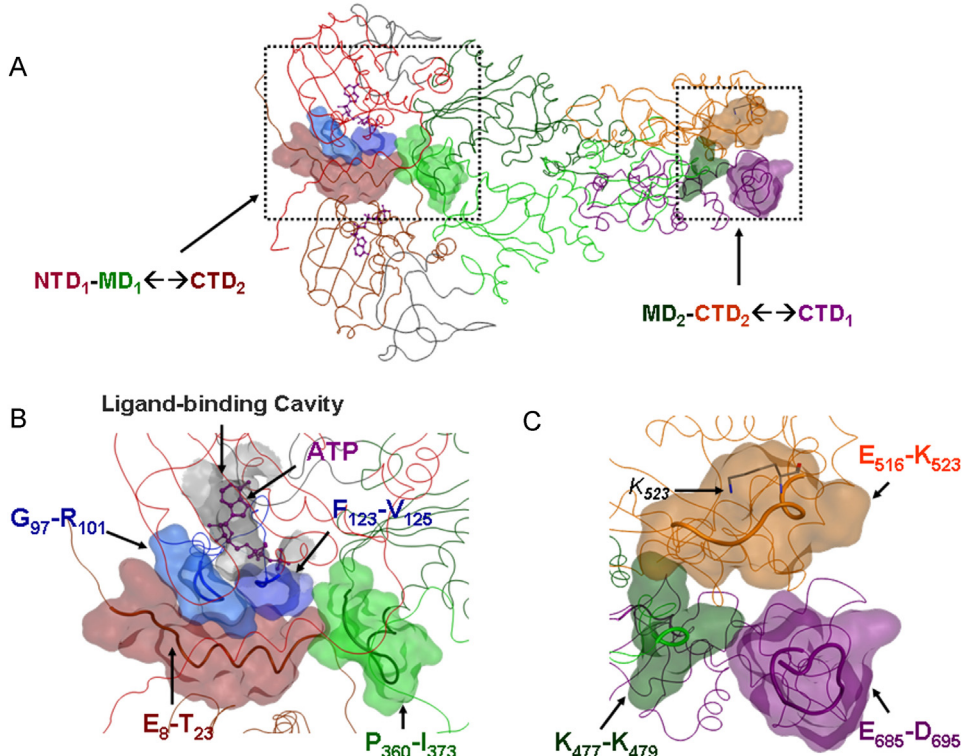


**Fig. 13.** Mutually stabilizing inter-chain contacts in the Hsp80Nc dimer model. (A) The relative positions of one out of each pair of symmetric and synergistic multi-domain contacts are highlighted in the dimer model. (B) The first of these two multi-domain contacts occurs between P<sub>360</sub>-I<sub>373</sub> from MD-A with E<sub>8</sub>-T<sub>23</sub> from NTD-B which in turn interacts with G<sub>97</sub>-R<sub>101</sub> and G<sub>123</sub>-V<sub>125</sub> from NTD-A, and vice versa. (C) The second multi-domain interaction occurs between K<sub>477</sub>-K<sub>479</sub> from MD-B and E<sub>685</sub>-D<sub>695</sub> from CTD-A which also interacts with E<sub>516</sub>-K<sub>523</sub> from CTD-B. Note: K<sub>523</sub> in Hsp80Nc corresponds to K<sub>560</sub> in human Hsp90α.

**Table 3**

Approximate calculated ligand binding energies for Hsp82Sc NTDs.

N-Terminal Domain	Calculated Binding Energy (kcal/mol)
ADP in <b>1amw</b> (open)	−29.5
ATP in <b>2cg9</b> (closed)	−13.6

absolute accuracy, being more suitable for comparison of relative ligand affinities rather than replication of the experimentally derived values. Hence we decided to validate the reliability and accuracy of our procedures and settings for docking ligands and calculations of their binding energies. The results demonstrated that the docking procedure consistently placed the physiological ligands (ADP and ATP) into the ligand-binding site, in **1amw** and **2cg9**, respectively; their top docked poses were virtually indistinguishable ( $\text{RMSD} < 0.2 \text{ \AA}$ ) from those witnessed in the experimentally determined structure (not shown). Validation of the procedure for ligand-binding energy calculations entailed comparison of the calculated binding energies of ADP in the 'open lid' form of the NTD (**1amw**) with ATP in the 'closed lid' form (**2cg9**). These initial results (Table 3) are consistent with experiments which show that Hsp82Sc has low intrinsic ATPase activity. The 'open lid', ADP-bound, form of the Hsp82Sc NTD has a more favorable calculated ligand-binding energy (−29.5 kcal/mol) than the 'closed lid' ATP-bound form (−13.6 kcal/mol) and would be the predominant configuration of that domain in the absence of activating co-chaperones. Since only the 'closed lid' form can perform ATP hydrolysis, Hsp82Sc should have low to non-existent intrinsic ATPase activity. It is possible that activating co-chaperones bind Hsp82Sc and cause some conformational changes which could either compensate for the adverse energetics of ATP binding or impose new energetic penalties on the 'open lid' form. The calculated ligand-binding energies for equivalent NTDs in Hsp80Nc (Table 4), however, exhibit a pattern distinct from that witnessed in the data in Table 3. The 'closed lid' ATP-bound form has a lower calculated ligand-binding energy (−32.8 kcal/mol) than the ADP bound 'open lid' form (−19.8 kcal/mol). Hence ATPase activity, which requires a closed lid, should be higher in Hsp80Nc. It should, therefore, not require an activating co-chaperone for the 'closed' lid form to be energetically favorable, relative to the 'open lid' form.

To further verify the validity of our method for calculating ligand-binding energy, we studied a mutation in Hsp82Sc (A107Q) known to increase intrinsic ATPase activity [38]. The calculated ligand-binding energy (−18.4 kcal/mol) for the 'closed lid' ATP-bound model of Hsp82Sc with the A107Q substitution is energetically superior to its native form (−13.6 kcal/mol). The calculated ligand-binding energy of the 'open lid' ADP-bound and substituted version is, however, almost identical (−29.7 kcal/mol) to its unsubstituted version (−29.5 kcal/mol). While the calculated ligand-binding energies still favor the 'open lid' ADP-bound form of the A107Q substitution over its 'closed lid' ATP-bound form, the reduction in energetic unfavorability for the 'closed lid' form would translate into an increase in intrinsic ATPase activity.

As stated in Section 1, we were interested in exploring whether the residue sequence differences in the 'lid' region might account for the higher intrinsic activity of Hsp80Nc vis-à-vis that of Hsp82Sc. To test this hypothesis, the ligand-binding energies for the ATP-bound 'closed lid' form for a number of in silico

**Table 5**Approximate calculated ligand binding energies for Hsp80Nc NTD Models with Residue Changes in the 'Lid' Region- $T_{98}\text{IARSGTKQFMEAL}_{111}$ .

Lid Sequence	Calculated Ligand Binding Energy for ATP (kcal/mol)
TIARSGTKQFMEAL	−32.8
TIARSGTKAFMEAL	−33.7
TIAKSGTKQFMEAL	−26.5
TIAKSGTKAFMEAL	−14.3

substitutions of Hsp80Nc and Hsp82Sc NTD models were calculated and compared. The main objective behind this approach was to convert the sequence of the Hsp80Nc lid to that of Hsp82Sc one substitution at a time and vice versa. The results of this exercise are presented in Table 5.

The calculated ligand-binding energies (Table 5), suggest that the dual substitution, R101 → K101 and Q106 → A106, which mimics the lid sequence of Hsp82Sc also end up almost reproducing its ligand-binding energy: −14.3 kcal/mol vs −13.6 kcal/mol. The ligand-binding energies of the ADP-bound 'open lid' form of the in silico substitutions shown in Table 5 fall within a narrow range—from −14.4 to −18.5 kcal/mol (not shown). The effects of *in silico* mutations on the calculated ligand-binding energy seem to be significantly larger in the ATP-bound 'closed lid' form of Hsp80Nc, as opposed to the ADP-bound 'open lid' form. It, therefore, follows that substitutions in the lid region of the Hsp82Sc which make it more like Hsp80Nc should result in an improvement in calculated ligand-binding energy of its 'closed lid' form with an almost negligible effect on the 'open lid' form. We tested this hypothesis by making a set of substituted ATP-bound 'closed lid' Hsp82Sc NTDs which progressively resembled Hsp80Nc. The results of this exercise are shown in Table 6 and confirm that this indeed is the case. It appears that the K98 → R98 and A103 → Q103 substitutions in Hsp82Sc do improve ligand-binding energy, with the latter substitution having the larger effect. The ADP-bound 'open lid' form of these substitutions (not shown) yielded ligand-binding energies in a narrow range (−30.0 to −31.5 kcal/mol) similar to that of native 'open lid' Hsp82Sc.

A comparison of all Hsp80Nc and Hsp82Sc models, included in Tables 5 and 6, was performed to understand the structural basis behind the effect of residue substitution in the 'lid' on calculated ligand-binding energy. It appears that changes in the overall pattern of hydrogen bonds between the 'lid' region and epitopes on the rim of the ligand-binding cavity comprise the most obvious difference between favorable and unfavorable residue substitutions, as depicted in Figs. 14 and 15.

Let us first consider the effects of residue substitutions in the 'lid' region of the NTD in Hsp80Nc. With its original sequence, the following residues in the 'lid' of the NTD (N<sub>94</sub>, N<sub>95</sub>, A<sub>100</sub>, R<sub>101</sub>, K<sub>105</sub>, Q<sub>106</sub>, T<sub>112</sub>, D<sub>116</sub>, S<sub>118</sub>) are involved in hydrogen bond interactions with residues (K<sub>45</sub>, Y<sub>48</sub>, E<sub>49</sub>, D<sub>91</sub>) on the rim of its ATP-binding site (Fig. 14A). Compared to native Hsp80Nc the R101 → K101 substitution (Fig. 14B) results in a measurable reduction in the number of interacting residues between the rim (K<sub>45</sub>, Y<sub>48</sub>, E<sub>49</sub>, D<sub>91</sub>) and 'lid' (N<sub>94</sub>, N<sub>95</sub>, K<sub>101</sub>, K<sub>105</sub>, Q<sub>106</sub>, T<sub>112</sub>). Substitution Q106 → A106 causes

**Table 6**Approximate calculated ligand binding energies for Hsp82Sc NTD Models with Residue Changes in the 'Lid' Region- $T_{95}\text{TIAKSGTKAFMEAL}_{108}$ .

Lid Sequence	Calculated Ligand Binding Energy (kcal/mol)
TIAKSGTKAFMEAL	−13.6
TIAKSGTKAFMEAL	−16.8
TIAKSGTKQFMEAL	−21.1
TIAKSGTKQFMEAL	−25.8

**Table 4**

Approximate calculated ligand binding energies for Hsp80Nc NTDs.

N-Terminal Domain	Calculated Binding Energy (kcal/mol)
Hsp80Nc ( <b>1amw</b> -based)	−19.8
Hsp80Nc ( <b>2cg9</b> -based)	−32.8

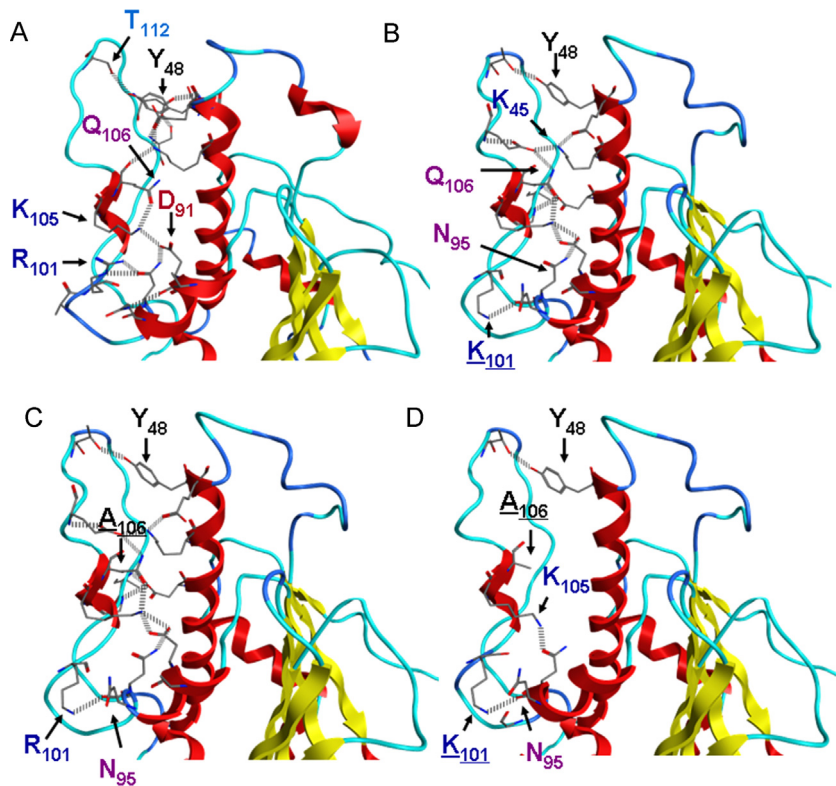


**Fig. 14.** Hydrogen bonds around the 'lid' region of the NTD in native Hsp80Nc and three substitutions progressively mimicking Hsp82Sc. (A) The unsubstituted native version of Hsp80Nc. (B) the first single-residue substitution, R101K, causes a slight decrease in the number of hydrogen bonds between the 'lid' and the rim of the ligand-binding cavity. (C) The second single-residue substitution, Q106A, has a similar effect albeit involving different residues. (D) The double substitution, R101K and Q106A, causes the largest decrease in the number of hydrogen bond interactions between the 'lid' and the rim.

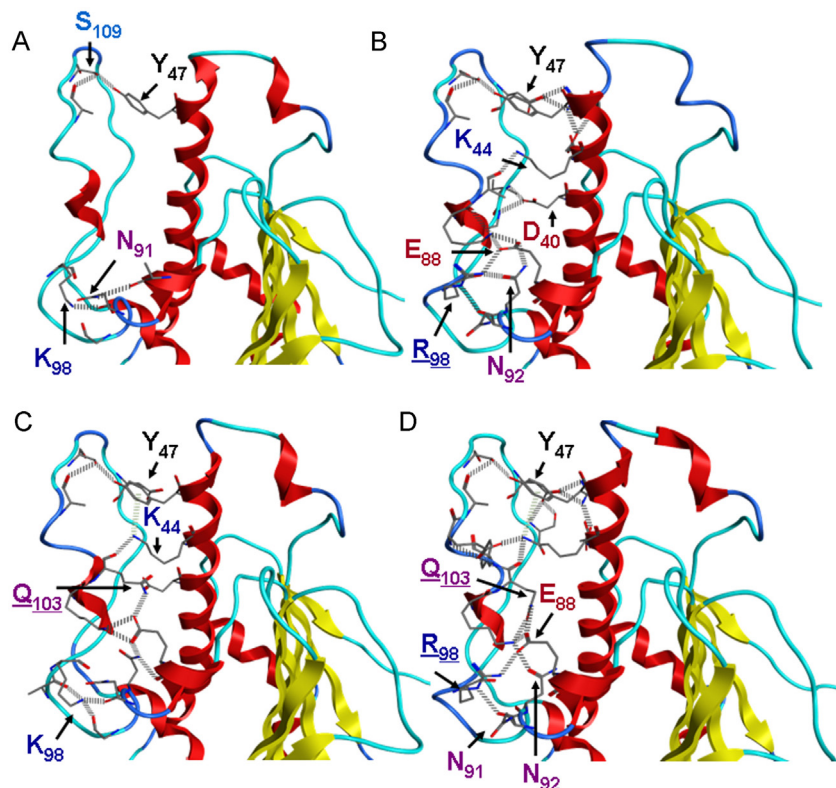


**Fig. 15.** Hydrogen bonds around the 'lid' region of the NTD in ligand-bound native form of Hsp82Sc and its three virtual mutations which progressively mimic Hsp80Nc. (A) the unsubstituted version of Hsp82Sc. (B) the first residue substitution, K98R, and the second one, A103Q. (C) result in a progressive increase in the number of hydrogen bonds between the 'lid' and the rim. (D) The double substituted version of Hsp82Sc, K98R and A103Q, which mimics the lid sequence of native Hsp80Nc, has pattern of hydrogen bond interactions almost identical to Hsp80Nc.

an even more pronounced reduction in the number of interacting residues in both the 'lid' region ( $N_{94}, R_{101}, K_{105}, A_{106}, T_{112}$ ) and the rim ( $K_{45}, R_{47}, Y_{48}, E_{49}$ ) as shown in Fig. 14C. The double substitution,  $R_{101} \rightarrow K_{101}$  and  $Q_{106} \rightarrow A_{106}$ , has the most dramatic effect on the number of hydrogen bond interactions between residues in the 'lid' and the rim and almost replicates that in Hsp82Sc (Fig. 14D). Only  $Y_{48}$  from the rim is involved in an interaction with  $T_{112}$  in the 'lid'. The remainder of the interacting residues ( $N_{94}, N_{95}, K_{101}, K_{105}, Q_{106}$ ) seem to form a localized hydrogen bond network which does not involve residues on the rim of the ligand-binding cavity.

Residue substitutions in Hsp82Sc exhibit the reverse pattern to that seen with Hsp80Nc. The NTD with the original sequence (Fig. 15A) displays sparse 'lid'-rim interactions, virtually identical to those seen in the double substituted Hsp80Nc ( $Y_{47}$  to  $S_{108}$ ). The  $K_{98} \rightarrow R_{98}$  substitution results in a moderate increase in interactions between the 'lid' ( $N_{90}, N_{91}, R_{98}, K_{102}, A_{103}, S_{108}$ ) and rim ( $D_{42}, Y_{47}, K_{48}, E_{88}$ ) as depicted in Fig. 15B. The  $A_{103} \rightarrow Q_{103}$  substitution (Fig. 15C) also improves interactions between residues in the 'lid' ( $N_{91}, N_{92}, A_{97}, K_{98}, K_{102}, Q_{103}, A_{106}, S_{108}, D_{112}$ ) and in the rim ( $D_{43}, K_{44}, Y_{47}, E_{88}$ ). The double substitution,  $K_{98} \rightarrow R_{98}$  and  $A_{103} \rightarrow Q_{103}$ , furthers this trend by creating a pattern of hydrogen-bond interactions between the lid and rim that is similar to that in Hsp80Nc (Fig. 15D). It appears that residue substitutions in the 'lid' region, which lead to the formation of more hydrogen bonds with the rim, improve the energetics for ATP binding. Furthermore, inverse substitution of equivalent residues results in a measurable decrease in the favorability of such interactions.

#### 4. Conclusions

Understanding the molecular mechanism responsible for the higher intrinsic activity of Hsp80Nc was one of the main objectives of the study described in this communication. While cochaperone-mediated modulation of ATPase activity in various Hsp90s has been the subject of extensive studies, differences in their intrinsic activity remain largely unexplored [11]. The decision to compare and contrast Hsp80Nc and Hsp82Sc was a follow up on previous research work by our group on Hsp80Nc [26–28,31,32]. Apparently a few differences in the residue sequence between the two proteins have a marked impact on intrinsic ATPase activity, in spite of the high degree of sequence and structural conservation of the major domains across eukaryotic species.

As described in Section 3, we were able to reconstruct full length models of Hsp80Nc and Hsp82Sc from homology-based models of individual domains and indirect experimental data based de novo reconstructions of inter-domain linkers. These models were evaluated for quality and found equivalent to experimentally determined structures of truncated Hsp90 constructs. We discovered a novel multi-domain interaction involving the MD and CTD from one chain (in a dimer) with the reconstructed CTD terminus from the other chain. This newly identified multi-domain interaction occurs near a residue ( $K_{523}$ ) equivalent to that in the human Hsp90 $\alpha$  ( $K_{560}$ ) known to bind to Novobiocin, a ligand of the secondary nucleoside binding site in the CTD [68]. The potential stabilizing effect of this novel interaction on the putative CTD ligand-binding site is strikingly similar to a multi-domain interaction at the other end of the dimer—between the NTD and MD from one chain and the NTD from the other chain.

While comparing the dimers of Hsp80Nc and Hsp82Sc to their monomers and to each other did provide novel insights into dimerization-induced structural changes, they gave little insight into the basis for differential intrinsic ATPase activity. A comparative study of binding energies of the physiological ligands at the active site of Hsp80Nc and Hsp82Sc was far more informative. It appears that a significant part of the differences between

the intrinsic activities of the two proteins is linked to the energetic favorability of their 'closed lid' (active) state versus the 'open lid' (inactive) state. The residue sequence of the lid region in Hsp80Nc contains two small, but important, changes from the default sequence found in most other Hsp90, including Hsp82Sc. These two substitutions ( $R_{101}$  and  $Q_{106}$  in Hsp80Nc) allow the formation of an extensive hydrogen bond network that stabilizes the 'closed' form of the lid by reducing or eliminating the energetic penalty for lid closure. Hence the lid region in Hsp80Nc is more likely to close spontaneously and hydrolyze the trapped ATP molecule in the active site than that in Hsp82Sc. A 'virtual' site-directed mutagenesis experiment verified that substitution of two residues at the equivalent positions in Hsp82Sc ( $K_{98} \rightarrow R_{98}$  and  $A_{103} \rightarrow Q_{103}$ ) led to a significant improvement in the energetic favorability of the 'closed lid' form. We have therefore identified a plausible molecular mechanism underlying the intrinsic activity of Hsp80Nc.

In the future, protein–protein docking will be used to explore the interactions of our homology-based Hsp80Nc models with endogenous co-chaperones and ancillary proteins. Homology-based models of full-length Hsp80Nc and Hsp82Sc will be useful in enhancing our understanding of the secondary nucleotide-binding site in the C-terminal domain as an experimentally determined structure with its ligands is currently unavailable. In addition, such models will permit exploration of the structural basis of the putative allosteric coupling between the primary and secondary nucleotide binding sites thereby leading to design of new inhibitors for Hsp90s.

#### Conflict of interest

The authors declare no competing financial interest.

#### Acknowledgements

This work was supported in part by an operating grant (to M.K.) from the Natural Sciences and Engineering Research Council of Canada. The authors are grateful to Dr. S.-L. Wong for reading the manuscript and providing valuable suggestions.

**Contributions:** SSR did the homology modeling, RWW purified the protein, MK and SSR designed the study and wrote the manuscript.

#### Appendix A. Supplementary data

Supplementary data associated with this article can be found, in the online version, at <http://dx.doi.org/10.1016/j.jmgm.2013.02.008>.

#### References

- [1] S. Lindquist, E.A. Craig, The heat-shock proteins, *Annual Review of Genetics* 22 (1988) 631–677.
- [2] R.M. Vabulas, S. Raychaudhuri, M. Hayer-Hartl, F.U. Hartl, Protein folding in the cytoplasm and the heat shock response, *Cold Spring Harbor Perspectives in Biology* 2 (2010) a004390.
- [3] W.B. Pratt, Y. Morishima, M. Murphy, M. Harrell, Chaperoning of glucocorticoid receptors, *Handbook of Experimental Pharmacology* 172 (2006) 111–138.
- [4] D.B. DeFranco, C. Ramakrishnan, Y. Tang, Molecular chaperones and subcellular trafficking of steroid receptors, *Journal of Steroid Biochemistry & Molecular Biology* 65 (1998) 51–58.
- [5] C. Garrido, C. Paul, R. Seigneuric, H.H. Kampinga, The small heat shock proteins family: The long forgotten chaperones, *The International Journal of Biochemistry & Cell Biology* 44 (2012) 1588–1592.
- [6] S. Salinthone, M. Tyagi, W.T. Gerthoffer, Small heat shock proteins in smooth muscle, *Pharmacology & Therapeutics* 119 (2008) 44–54.
- [7] E. Laskowska, E. Matuszewska, D. Kuczyńska-Wiśniewska, Small heat shock proteins and protein-misfolding diseases, *Current Pharmaceutical Biotechnology* 11 (2010) 146–157.

- [8] F. Hennessy, W.S. Nicoll, R. Zimmermann, M.E. Cheetham, G.L. Blatch, Not all J domains are created equal: implications for the specificity of Hsp40-Hsp70 interactions, *Protein Science* 14 (2005) 1697–1709.
- [9] C. Didelot, E. Schmitt, M. Brunet, L. Maingret, A. Parcellier, C. Garrido, Heat shock proteins: endogenous modulators of apoptotic cell death, *The Handbook of Experimental Pharmacology* 172 (2006) 171–198.
- [10] R.E. Wang, Targeting heat shock proteins 70/90 and proteasome for cancer therapy, *Current Medicinal Chemistry* 18 (2011) 4250–4264.
- [11] R. Zhao, W.A. Houry, Molecular interaction network of the Hsp90 chaperone system, *Advances in Experimental Medicine and Biology* 594 (2007) 27–36.
- [12] L. Shaner, K.A. Morano, All in the family: atypical Hsp70 chaperones are conserved modulators of Hsp70 activity, *Cell Stress and Chaperones* 12 (2007) 1–8.
- [13] P. Csermely, T. Schnaider, C. Söti, Z. Prohászka, G. Nardai, The 90-kDa molecular chaperone family: structure, function, and clinical applications. A comprehensive review, *Pharmacology & Therapeutics* 79 (1998) 129–168.
- [14] J.S. Hahn, The Hsp90 chaperone machinery: from structure to drug development, *BMB Report* 42 (2009) 623–630.
- [15] A.T. Large, M.D. Goldberg, P.A. Lund, Chaperones and protein folding in the archaea, *Biochemical Society Transactions* 37 (2009) 46–51.
- [16] B. Panaretou, C. Prodromou, S.M. Roe, R. O'Brien, J.E. Ladbury, P.W. Piper, L.H. Pearl, ATP binding and hydrolysis are essential to the function of the Hsp90 molecular chaperone in vivo, *EMBO Journal* 17 (1998) 4829–4836.
- [17] P. Csermely, C.R. Kahn, The 90-kDa heat shock protein (hsp-90) possesses an ATP binding site and autophosphorylating activity, *Journal of Biological Chemistry* 266 (1991) 4943–4950.
- [18] C. Prodromou, S.M. Roe, R. O'Brien, J.E. Ladbury, P.W. Piper, L.H. Pearl, Identification and structural characterization of the ATP/ADP-binding site in the Hsp90 molecular chaperone, *Cell* 90 (1997) 65–75.
- [19] C. Söti, A. Vermes, T.A. Haystead, P. Csermely, Comparative analysis of the ATP-binding sites of Hsp90 by nucleotide affinity cleavage: a distinct nucleotide specificity of the C-terminal ATP-binding site, *European Journal of Biochemistry* 270 (2003) 2421–2428.
- [20] C. Garnier, D. Lafitte, P.O. Tsvetkov, P. Barbier, J. Leclerc-Devin, J.M. Millot, C. Briand, A.A. Makarov, M.G. Catelli, V. Peyrot, Binding of ATP to heat shock protein 90: evidence for an ATP-binding site in the C-terminal domain, *Journal of Biological Chemistry* 277 (2002) 12208–12214.
- [21] T. Langer, H. Schlatter, H. Fasold, Evidence that the novobiocin-sensitive ATP-binding site of the heat shock protein 90 (hsp90) is necessary for its autophosphorylation, *Cell Biology International* 26 (2002) 653–657.
- [22] R.J. Schumacher, W.J. Hansen, B.C. Freeman, E. Alnemri, G. Litwack, D.O. Toft, Cooperative action of Hsp70, Hsp90, and Dnaj proteins in protein renaturation, *Biochemistry* 35 (1996) 14889–14898.
- [23] S. Tsutsumi, K. Beebe, L. Neckers, Impact of heat-shock protein 90 on cancer metastasis, *Future Oncology* 5 (2009) 679–688.
- [24] C. Söti, L. Radics, I. Yahara, P. Csermely, Interaction of vanadate oligomers and permolybdate with the 90-kDa heat-shock protein Hsp90, *European Journal of Biochemistry* 255 (1998) 611–617.
- [25] G. Chiosis, E. Caldas-Lopes, D. Solit, Heat shock protein-90 inhibitors: a chronicle from geldanamycin to today's agents, *Current Opinion in Investigational Drugs* 7 (2006) 534–541.
- [26] D.G. Freitag, P.M. Ouimet, T.L. Girvitz, M. Kapoor, Heat shock protein 80 of *Neurospora crassa*, a cytosolic molecular chaperone of the eukaryotic stress 90 family, interacts directly with heat shock protein 70, *Biochemistry* 36 (1997) 10221–10229.
- [27] T.L. Girvitz, P.M. Ouimet, M. Kapoor, Heat shock protein 80 of *Neurospora crassa*: sequence analysis of the gene and expression during the asexual phase, *Canadian Journal of Microbiology* 46 (2000) 981–991.
- [28] P.M. Ouimet, M. Kapoor, Nucleotide binding and hydrolysis properties of *Neurospora crassa* cytosolic molecular chaperones, Hsp70 and Hsp80, heat-inducible members of the eukaryotic stress-70 and stress-90 families, *Biochemistry & Cell Biology* (1999) 89–99.
- [29] B.A.L. Owen, W.P. Sullivan, S.J. Felts, D.O. Toft, Regulation of heat shock protein 90 ATPase activity by sequence in the carboxy terminus, *Journal of Biological Chemistry* 277 (2002) 7086–7091.
- [30] S.H. McLaughlin, H.W. Smith, S.E. Jackson, Stimulation of the weak ATPase activity of human Hsp90 by a client protein, *Journal of Molecular Biology* 315 (2002) 785–798.
- [31] P.M. Ouimet, M. Kapoor, Analysis of complex formation between Hsp80 and Hsp70, cytosolic molecular chaperones of *Neurospora crassa*, by enzyme-linked immunosorbent assays (ELISA), *Biochemistry & Cell Biology* 76 (1998) 97–106.
- [32] M.E. Britton, M. Kapoor, The oligomeric state, complex formation, and chaperoning activity of hsp70 and hsp80 of *Neurospora crassa*, *Biochemistry & Cell Biology* 80 (2002) 797–809.
- [33] M.M. Ali, S.M. Roe, C.K. Vaughan, P. Meyer, B. Panaretou, P.W. Piper, C. Prodromou, L.H. Pearl, Crystal structure of an Hsp90-nucleotide-p23/Sba1 closed chaperone complex, *Nature* 440 (2006) 1013–1017.
- [34] P. Bron, E. Giudice, J.P. Rolland, R.M. Buey, P. Barbier, J.F. Díaz, V. Peyrot, D. Thomas, C. Garnier, Apo-Hsp90 coexists in two open conformational states in solution, *Biology of Cell* 100 (2008) 413–425.
- [35] D.R. Southworth, D.A. Agard, Client-loading conformation of the Hsp90 molecular chaperone revealed in the cryo-EM structure of the human Hsp90: Hop complex, *Molecular Cell* 42 (2011) 771–781.
- [36] P. Csermely, J. Kajtár, M. Hollósi, G. Jalszovszky, S. Holly, C.R. Kahn, P. Gergely, C. Söti, K. Mihály, J. Somogyi, ATP induces a conformational change of the 90-kDa heat shock protein (hsp90), *Journal of Biological Chemistry* 268 (1993) 1901–1907.
- [37] G. Siligardi, B. Hu, B. Panaretou, P.W. Piper, L.H. Pearl, C. Prodromou, Co-chaperone regulation of conformational switching in the Hsp90 ATPase cycle, *Journal of Biological Chemistry* 279 (2004) 51989–51998.
- [38] C.N. Cunningham, K.A. Krukenberg, D.A. Agard, Intra- and intermonomer interactions are required to synergistically facilitate ATP hydrolysis in Hsp90, *Journal of Biological Chemistry* 283 (2008) 21170–21178.
- [39] C. Söti, A. Rácz, P. Csermely, A nucleotide-dependent molecular switch controls ATP binding at the C-terminal domain of Hsp90, N-terminal nucleotide binding unmasks a C-terminal binding pocket, *Journal of Biological Chemistry* 277 (2002) 7066–7075.
- [40] K.A. Krukenberg, T.O. Street, L.A. Lavery, D.A. Agard, Conformational dynamics of the molecular chaperone Hsp90, *Quarterly Reviews of Biophysics* 44 (2011) 229–255.
- [41] M.A. Martinez-Yamout, R.P. Venkitakrishnan, N.E. Preece, G. Kroon, P.E. Wright, H.J. Dyson, Localization of sites of interaction between p23 and Hsp90 in solution, *Journal of Biological Chemistry* 281 (2006) 14457–14464.
- [42] M. Retzlaff, F. Hagn, L. Mitschke, M. Hessling, F. Gugel, H. Kessler, K. Richter, J. Buchner, Asymmetric activation of the hsp90 dimer by its cochaperone aha1, *Molecular Cell* 37 (2010) 344–354.
- [43] O. Hainzl, M.C. Lapina, J. Buchner, K. Richter, The charged linker region is an important regulator of Hsp90 function, *Journal of Biological Chemistry* 284 (2009) 22559–22567.
- [44] S. Tsutsumi, M. Mollapour, C. Prodromou, C.T. Lee, B. Panaretou, S. Yoshida, M.P. Mayer, L.M. Neckers, Charged linker sequence modulates eukaryotic heat shock protein 90 (Hsp90) chaperone activity, *Proceedings of National Academy of Sciences of United States of America* 109 (2012) 2937–2942.
- [45] C. Prodromou, B. Panaretou, S. Chohan, G. Siligardi, R. O'Brien, J.E. Ladbury, M.S. Roe, P.W. Piper, L.H. Pearl, The ATPase cycle of Hsp90 drives a molecular 'clamp' via transient dimerization of the N-terminal domains, *The EMBO Journal* 19 (2000) 4383–4392.
- [46] Molecular Operating Environment, version 2008.10, Chemical Computing Group Inc., Montreal, PQ.
- [47] T.A. Halgren, The merck molecular force field. I. Basis, form, scope, parametrization, and performance of MMFF94, *Journal of Computational Chemistry* 17 (1996) 490–519.
- [48] The National Center for Biotechnology Information, <http://www.ncbi.nlm.nih.gov/> (last accessed on Nov. 15, 2012).
- [49] S. Henikoff, J. Henikoff, Amino acid substitution matrices from protein blocks, *Proceedings of National Academy of Sciences of United States of America* 89 (1992) 10915–10919.
- [50] M. Feher, E. Deretey, S. Roy, BHB: A simple knowledge-based scoring function to improve the efficiency of database screening, *Journal of Chemical Information & Computer Sciences* 43 (2003) 1316–1327.
- [51] J.M. Schmidt, J. Mercure, G.B. Tremblay, M. Pagé, A. Kalbalkji, M. Feher, R. Dunn-Dufault, M.G. Peter, P.R. Redden, De novo design, synthesis, and evaluation of novel nonsteroidal phenanthrene ligands for the estrogen receptor, *Journal of Medicinal Chemistry* 46 (2003) 1408–1418.
- [52] S.W. Provencher, J. Glockner, Estimation of globular protein secondary structure from circular dichroism, *Biochemistry* 20 (1981) 33–37.
- [53] L. Whitmore, B.A. Wallace, Biopolymers protein secondary structure analyses from circular dichroism spectroscopy: methods and reference databases, *Biopolymers* 89 (2008) 392–440.
- [54] A.K. Shiu, S.F. Harris, D.R. Southworth, D.A. Agard, Structural analysis of *E. coli* hsp90 reveals dramatic nucleotide-dependent conformational rearrangements, *Cell* 127 (2006) 329–340.
- [55] D.E. Dollins, R.M. Immormino, D.T. Gewirth, Structure of unliganded GRP94, the endoplasmic reticular Hsp90. Basis for nucleotide-induced conformational change, *Journal of Biological Chemistry* 280 (2005) 30438–30447.
- [56] M. Zhang, M. Boter, K. Li, Y. Kadota, B. Panaretou, C. Prodromou, K. Shirasu, L.H. Pearl, Structural and functional coupling of hsp90- and sgt1-centred multi-protein complexes, *EMBO Journal* 27 (2008) 2789–2798.
- [57] W.M. Obermann, H. Sondermann, A.A. Russo, N.P. Pavletich, F.U. Hartl, In vivo function of Hsp90 is dependent on ATP binding and ATP hydrolysis, *Journal of Cell Biology* 143 (1998) 901–910.
- [58] K.D. Corbett, J.M. Berger, Structure of the ATP-binding domain of *Plasmodium falciparum* Hsp90, *Proteins* 78 (2010) 2738–2744.
- [59] J.P. Grenert, W.P. Sullivan, P. Fadden, T.A. Haystead, J. Clark, E. Mimnaugh, H. Krutzsch, H.J. Ochel, T.W. Schulte, E. Sausville, L.M. Neckers, D.O. Toft, The amino-terminal domain of heat shock protein 90 (hsp90) that binds geldanamycin is an ATP/ADP switch domain that regulates hsp90 conformation, *Journal of Biological Chemistry* 272 (1997) 23843–23850.
- [60] G.E. Karagöz, A.M. Duarte, H. Ippel, C. Uetrecht, T. Sinnige, M. van Rosmalen, J. Hausmann, A.J. Heck, R. Boelens, S.G. Rüdiger, N-terminal domain of human Hsp90 triggers binding to the cochaperone p23, *Proceedings of National Academy of Sciences of United States of America* 108 (2011) 580–585.
- [61] K. Richter, S. Moser, F. Hagn, R. Friedrich, O. Hainzl, M. Heller, S. Schlee, H. Kessler, J. Reinstein, J. Buchner, Intrinsic inhibition of the Hsp90 ATPase activity, *Journal of Biological Chemistry* 281 (2006) 11301–11311.
- [62] M. Wiederstein, M.J. Sippl, ProSA-web: interactive web service for the recognition of errors in three-dimensional structures of proteins, *Nucleic Acids Research* 35 (2007) W407–W410.
- [63] W.M. Rockey, A.H. Elcock, Structure selection for protein kinase docking and virtual screening: homology models or crystal structures? *Current Protein & Peptide Science* 7 (2006) 437–457.

- [64] I. Motto, A. Bordogna, A.A. Soshilov, M.S. Denison, L. Bonati, New aryl hydrocarbon receptor homology model targeted to improve docking reliability, *Journal of Chemical Information & Modelling* 51 (2011) 2868–2881.
- [65] J. Carlson, R.G. Coleman, V. Setola, J.J. Irwin, H. Fan, A. Schlessinger, A. Sali, B.L. Roth, B.K. Shoichet, Ligand discovery from a dopamine D3 receptor homology model and crystal structure, *Nature Chemical Biology* 7 (2011) 69–78.
- [66] K.A. Krukenberg, F. Förster, L.M. Rice, A. Sali, D.A. Agard, Multiple conformations of *E. coli* Hsp90 in solution: insights into the conformational dynamics of Hsp90, *Structure* 16 (2008) 755–765.
- [67] DichroWeb, <http://dichroweb.cryst.bbk.ac.uk/html/home.shtml> (last accessed on Nov. 15, 2012).
- [68] R.L. Matts, A. Dixit, L.B. Peterson, L. Sun, S. Voruganti, P. Kalyanaraman, S.D. Hartson, G.M. Verkhivker, B.S. Blagg, Elucidation of the Hsp90 C-terminal inhibitor binding site, *ACS Chemical Biology* 6 (9) (2011) 800–807.
- [69] L. Moullintraffort, M. Bruneaux, A. Nazabal, D. Allegro, E. Giudice, F. Zal, V. Peyrot, P. Barbier, D. Thomas, C. Garnier, Biochemical and biophysical characterization of the Mg<sup>2+</sup>-induced 90-kDa heat shock protein oligomers, *Journal of Biological Chemistry* 285 (2010) 15100–15110.
- [70] D.R. Southworth, D.A. Agard, Species-dependent ensembles of conserved conformational states define the Hsp90 chaperone ATPase cycle, *Molecular Cell* 32 (2008) 631–640.